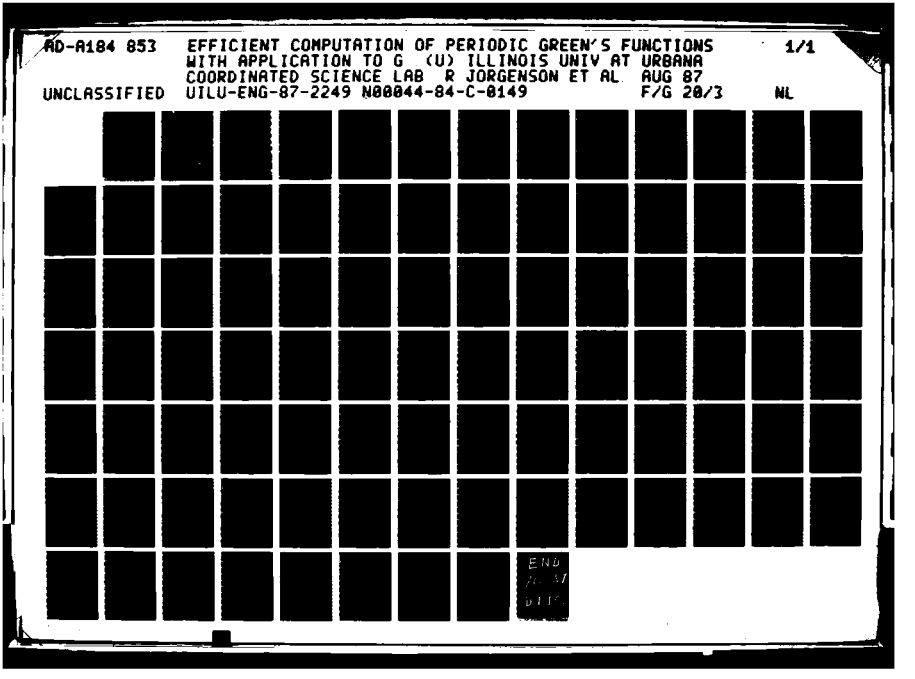
AD-A184 853 EFFICIENT COMPUTATION OF PERIODIC GREEN'S FUNCTIONS WITH APPLICATION TO G (U) ILLINOIS UNIV AT URBANA COORDINATED SCIENCE LAB R JORGENSON ET AL AUG 87
1/1
UNCLASSIFIED UILU-ENG-87-2249 N00044-84-C-0149 F/G 20/3 NL
END
DTIC

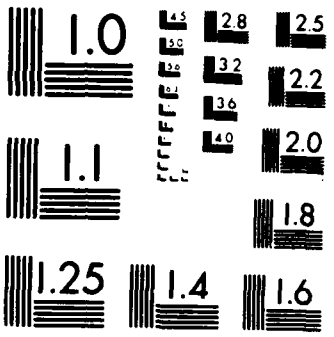

August 1987 UILU-ENG-87-2249

COORDINATED SCIENCE LABORATORY
College of Engineering

EFFICIENT COMPUTATION OF PERIODIC GREEN'S FUNCTIONS WITH APPLICATION TO GRATING STRUCTURES

R. Jorgenson
R. Mittra

UNIVERSITY OF ILLINOIS AT URBANA-CHAMPAIGN

UNCLASSIFIED
SECURITY CLASSIFICATION OF THIS PAGE

ADA184853

REPORT DOCUMENTATION PAGE

1a. REPORT SECURITY CLASSIFICATION Unclassified	1b. RESTRICTIVE MARKINGS None
2a. SECURITY CLASSIFICATION AUTHORITY	3. DISTRIBUTION/AVAILABILITY OF REPORT Approved for public release; distribution unlimited
2b. DECLASSIFICATION/DOWNGRADING SCHEDULE	
4. PERFORMING ORGANIZATION REPORT NUMBER(S) UILU-ENG-87-2249	5. MONITORING ORGANIZATION REPORT NUMBER(S)
6a. NAME OF PERFORMING ORGANIZATION Coordinated Science Lab University of Illinois	6b. OFFICE SYMBOL (If applicable) N/A
	7a. NAME OF MONITORING ORGANIZATION Office of Naval Research
6c. ADDRESS (City, State, and ZIP Code) 1101 W. Springfield Ave. Urbana, IL 61801	7b. ADDRESS (City, State, and ZIP Code) 800 N. Quincy St. Arlington, VA 22217
8a. NAME OF FUNDING/SPONSORING ORGANIZATION Joint Services Electronics Program	8b. OFFICE SYMBOL (If applicable)
	9. PROCUREMENT INSTRUMENT IDENTIFICATION NUMBER N00014-84-C-0149
8c. ADDRESS (City, State, and ZIP Code) 800 N. Quincy St. Arlington, VA 22217	10. SOURCE OF FUNDING NUMBERS PROGRAM ELEMENT NO. / PROJECT NO. / TASK NO. / WORK UNIT ACCESSION NO.

11. TITLE (Include Security Classification)
Efficient Computation of Periodic Green's Functions with Application to Grating Structures.

12. PERSONAL AUTHOR(S)
Jorgenson, Roy and Mittra, Raj

13a. TYPE OF REPORT	13b. TIME COVERED	14. DATE OF REPORT (Year, Month, Day)	15. PAGE COUNT
Technical	FROM _____ TO _____	August 1987	88

16. SUPPLEMENTARY NOTATION

17. COSATI CODES			18. SUBJECT TERMS (Continue on reverse if necessary and identify by block number)
FIELD	GROUP	SUB-GROUP	Grating Structures; Acceleration of Summation; Poisson Summation; Periodic Green's Function; Strip Arrays; Frequency Selective Surface

19. ABSTRACT (Continue on reverse if necessary and identify by block number)

It is shown that electromagnetic scattering from periodic structures may be formulated in terms of an integral equation that has as its kernel a periodic Green's function. The periodic Green's function may be derived from two points of view: as a response to an array of line/point sources (spatial domain) or as a response from a series of current sheets (spectral domain). These responses are a Fourier transform pairand are slowly convergent summations. The convergence problems in each domain arise from unavoidable singularities in the reciprocal domain. A method is discussed to overcome the slow convergence by using the Poisson summation formula and summing in a combination of spectral and spatial domains. A parameter study is performed to determine an optimum way to weight the combination of domains. Simple examples of scattering from a one-dimensional array of strips and two-dimensional array of plates are used to illustrate the concepts.

20. DISTRIBUTION/AVAILABILITY OF ABSTRACT	21. ABSTRACT SECURITY CLASSIFICATION
☒ UNCLASSIFIED/UNLIMITED ☐ SAME AS RPT. ☐ DTIC USERS	Unclassified
22a. NAME OF RESPONSIBLE INDIVIDUAL	22b. TELEPHONE (Include Area Code) / 22c. OFFICE SYMBOL

DD FORM 1473, 84 MAR — 83 APR edition may be used until exhausted. All other editions are obsolete.

SECURITY CLASSIFICATION OF THIS PAGE
UNCLASSIFIED

EFFICIENT COMPUTATION OF PERIODIC GREEN'S FUNCTIONS

WITH APPLICATION TO GRATING STRUCTURES

By

Roy Jorgenson and Raj Mittra
University of Illinois
Urbana, IL

A-1

ABSTRACT

It is shown that electromagnetic scattering from periodic structures may be formulated in terms of an integral equation that has as its kernel a periodic Green's function. The periodic Green's function may be derived from two points of view: as a response to an array of line/point sources (spatial domain) or as a response from a series of current sheets (spectral domain). These responses are a Fourier transform pair and are slowly convergent summations. The convergence problems in each domain arise from unavoidable singularities in the reciprocal domain. A method is discussed to overcome the slow convergence by using the Poisson summation formula and summing in a combination of spectral and spatial domains. A parameter study is performed to determine an optimum way to weight the combination of domains. Simple examples of scattering from a one-dimensional array of strips and two-dimensional array of plates are used to illustrate the concepts.

TABLE OF CONTENTS

LIST OF FIGURES

1. INTRODUCTION

The interaction of electromagnetic fields with periodic structures has always proven difficult to analyze. Some examples of these structures include frequency selective surfaces [1], microstrip arrays [2] and sources inside waveguides [3]. One fruitful approach toward solving periodic problems involves the formulation of an integral equation and its numerical solution via the Method of Moments. The integral equation has as its kernel a periodic Green's function, which is, unfortunately, a slowly convergent summation. Consequently, the computer time required to solve the problem by the Method of Moments is dominated by the time needed to compute the impedance matrix elements.

In the past, investigators have used various techniques to speed convergence of the summation. Functions with a wide support in the spatial domain have been used as basis and testing functions to make the summations in the spectral domain more convergent [4,5]. Poisson's summation formula [6] has been used to speed convergence using a spatial domain approach [3,7] or using a spectral domain approach [2,8,9].

This report investigates the efficient computation of the periodic Green's functions to tie together the methods discussed in the preceding paragraph. Two examples of periodic problems are used for illustration. The first example, discussed in Chapter 2, is that of electromagnetic scattering from a strip grating with the strips arbitrarily rotated with respect to the $\hat{x}$ axis as shown in Figure 2.1. The periodic Green's function for this example involves a single summation. This simpler problem will be used to demonstrate the manner in which the periodic Green's function arises in the problem formulation, the slow convergence of the summation and a method of accelerating the convergence through use of Poisson's summation formula. Results will be presented to clarify specific points of the problem and to show how optimum parameters are chosen in order to maximize computational efficiency.

In Chapter 3, an extension of the techniques developed in Chapter 2 is applied to a two-dimensional array of plates on a skewed coordinate system as shown in Figure 3.1. The periodic Green's function arising in the plate array problem involves a double summation and is computationally more intensive than the strip array case. However, the behavior of the two-dimensional summation is similar to the behavior of the one-dimensional periodic Green's function. The conclusions of this study are summarized in Chapter 4.

2. THE ONE-DIMENSIONAL ARRAY

2.1 Introduction

In this chapter, the integral equation formulation for scattering from the strip grating shown in Figure 2.1 will be examined. The strips are rotated to make an angle θ with respect to the $\hat{x}$ axis. The strips are perfect electric conductors and are spaced b meters apart. The incident field is a plane wave where the direction of propagation in the xy plane makes an angle of θ_i with the $\hat{y}$ axis. The plane wave is either transverse magnetic (TM) to $\hat{z}$ or transverse electric (TE) to $\hat{z}$.

The case of plane wave incidence is the basis for analyzing all problems involving scattering from a periodic structure. If an arbitrary field (not a plane wave) is incident on a periodic structure, no relationship exists between the currents of different unit cells in the structure. Therefore, the currents on the entire structure must be treated as unknowns in a Moment Method solution. On the other hand, if the incident field is a plane wave, then a relationship may be found between currents of different unit cells based on Floquet's theorem; only the currents in a single unit cell must be treated as unknowns. This is discussed in more detail in Section 2.3. The response due to an arbitrary source is found by decomposing the arbitrary source into plane waves and adding the plane wave responses.

2.2 Definitions of Terms

In the remainder of this report, the Fourier transform is used extensively. The Fourier transform pair for the one-dimensional case is defined as

$$\tilde{F}(\beta_x) = \int_{-\infty}^{+\infty} f(x) e^{-j\beta_x x} dx \tag{2.1a}$$

$$f(x) = \frac{1}{2\pi} \int_{-\infty}^{+\infty} \tilde{F}(\beta_x) e^{+j\beta_x x} d\beta_x \tag{2.1b}$$

where f(x) is a function in the space domain and $\tilde{F}(\beta_x)$ is the Fourier transform of f(x) into the spectral domain.

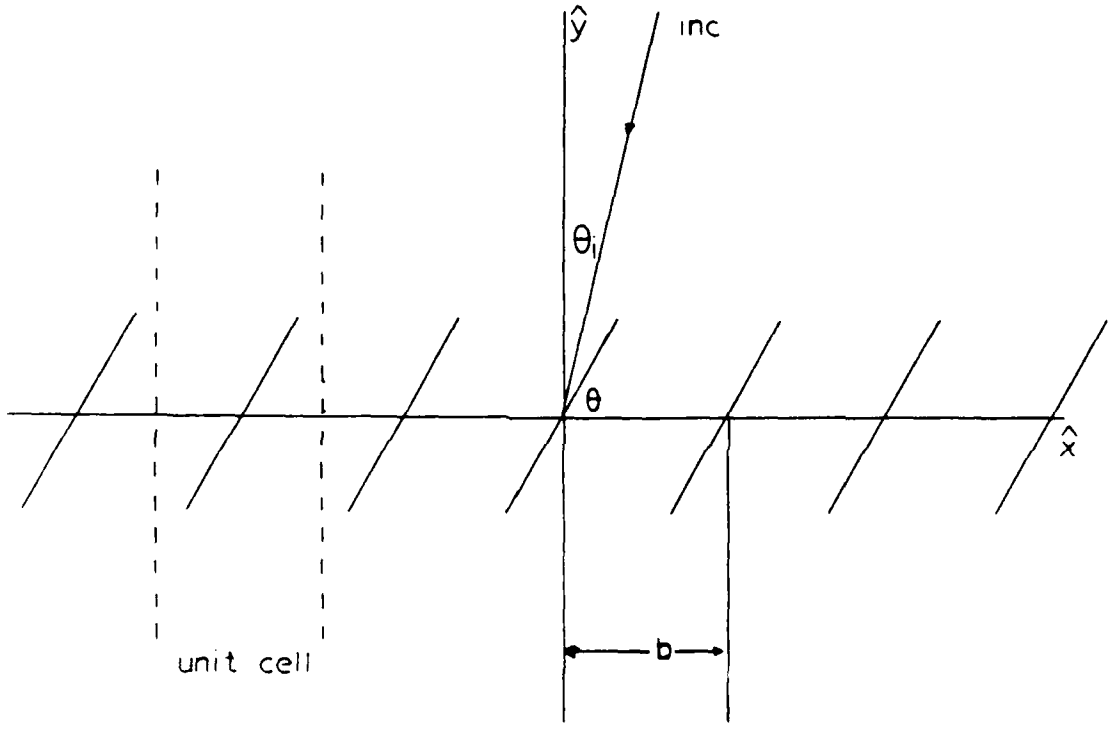

Figure 2.1 One-dimensional array geometry

The Fourier transform defined above is used in this report to transform periodic functions in the space domain into their equivalent representations in the spectral domain. A periodic function may be viewed as a convolution of the function truncated to one period with a comb function in space [10], i.e.,

$$f_p(x) = f(x) * \sum_{m=-\infty}^{\infty} \delta(x - mb) \tag{2.2}$$

where

$$f(x) = f_p(x) \quad \text{for } -\frac{b}{2} < x < +\frac{b}{2}$$

$$= 0 \quad \textit{otherwise} .$$

b is the period of $F_p(x)$ and * denotes the convolution operation defined as

$$f(x) * g(x) = \int_{-\infty}^{\infty} f(x')g(x - x')dx' \tag{2.3}$$

Since the Fourier transform of a comb function is also a comb function, albeit with a different period, and the transform of a convolution is the product of the transforms, the Fourier transform of Equation (2.2) is a function sampled at discrete values in the spectral domain.

$$\tilde{F}_p(\beta_x) = \tilde{F}(\beta_x) \sum_{m=-\infty}^{\infty} \delta\left(k - \frac{2\pi m}{b}\right) \tag{2.4}$$

A concise way to predict the location of the spectral domain comb components of Equation (2.4) given the location of the spatial domain comb components is through the use of a reciprocal lattice.

A periodic geometry has associated with it a spatial lattice and a reciprocal lattice [11]. The spatial lattice is a periodic arrangement of points in space and is formed by adding an integer number (m) of primitive vectors ($\hat{S}_1$) to a location $\vec{r}$. For the one-dimensional case under consideration, $\hat{S}_1 = b\hat{x}$ as shown in Figure 2.2.

$$\vec{r}' = \vec{r} + m\hat{S}_1 \tag{2.5}$$

$$= \vec{r} + mb\hat{x}$$

The overall periodic structure is formed when the unit cell, shown in Figure 2.1, is attached to each lattice point. The unit cell is defined as the smallest part of the structure that, when repeated, makes up the overall structure.

The reciprocal lattice is associated with the spectral domain just as the spatial lattice is associated with the spatial domain. The reciprocal lattice predicts where the discrete components of $\tilde{F}(\beta_x)$ are located in the spectral domain. In the one-dimensional case under consideration, the reciprocal lattice is defined by adding an integer number (n) of primitive reciprocal vectors ($\tilde{S}_1$) to a location in the spectral domain ($\vec{k}$)

$$\vec{K}' = \vec{k} + n\tilde{S}_1 \tag{2.6}$$

where $\tilde{S}_1$ is related to the spatial primitive lattice vector by

$$\hat{S}_1 \cdot \tilde{S}_1 = 2\pi \tag{2.7}$$

Therefore,

$$\tilde{S}_1 = \frac{2\pi}{b}\hat{x} \tag{2.8}$$

The reciprocal lattice corresponding to the spatial lattice of Figure 2.2 is shown in Figure 2.3.

The concept of the reciprocal lattice is not too useful for the one-dimensional case. However, for two-dimensional periodicity on skewed coordinates discussed in Chapter 3, it provides great insight. Derivation of the two-dimensional reciprocal lattice will be deferred until Chapter 3.

2.3 Formulation of G_p

The electric field integral equation will be used to solve the one-dimensional strip array problem. Using the fact that the tangential E field is zero on the strip, the following equation is obtained:

$$\hat{n} \times \left[-j\omega\mu \int \vec{J}(s')G_p(s,s')ds' + \frac{1}{j\omega\epsilon} \nabla \int \nabla' \cdot \vec{J}(s')G_p(s,s')ds' \right] = -\hat{n} \times \vec{E}_{inc}(s) \tag{2.9}$$

where G_p is the periodic Green's function and $\vec{J}$ is the surface current density flowing in a

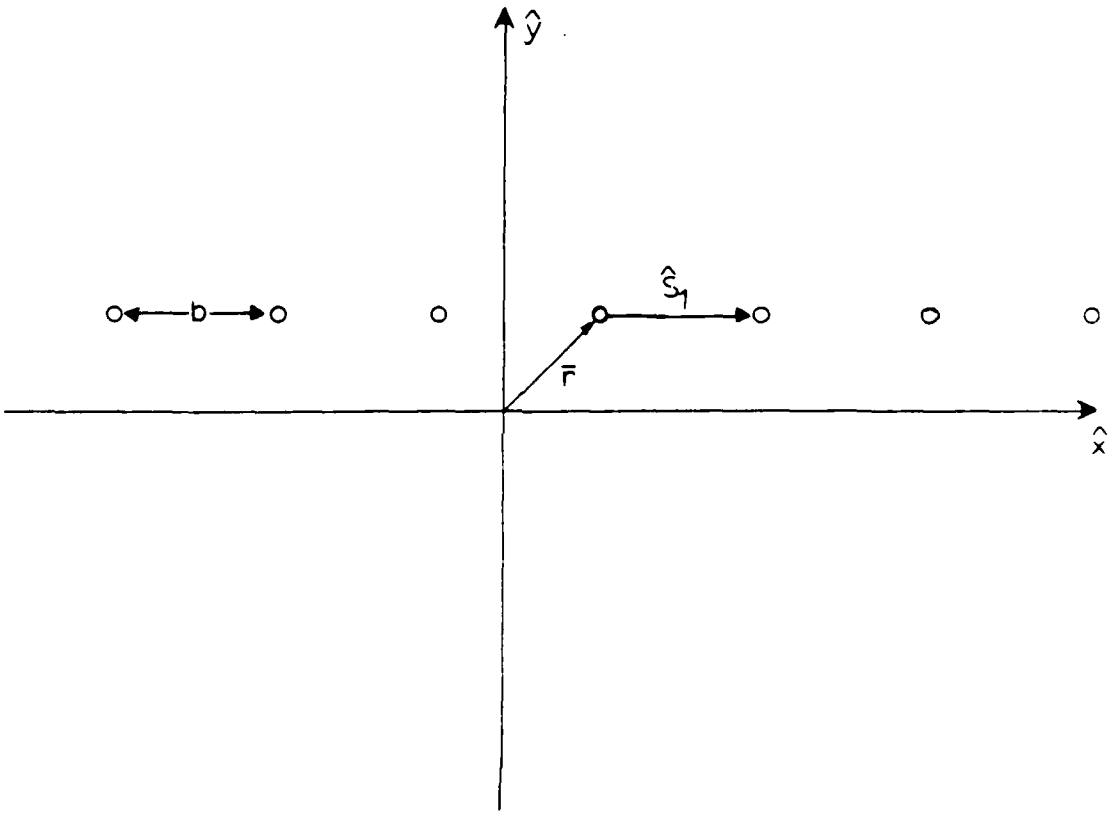

Figure 2.2 One-dimensional spatial lattice

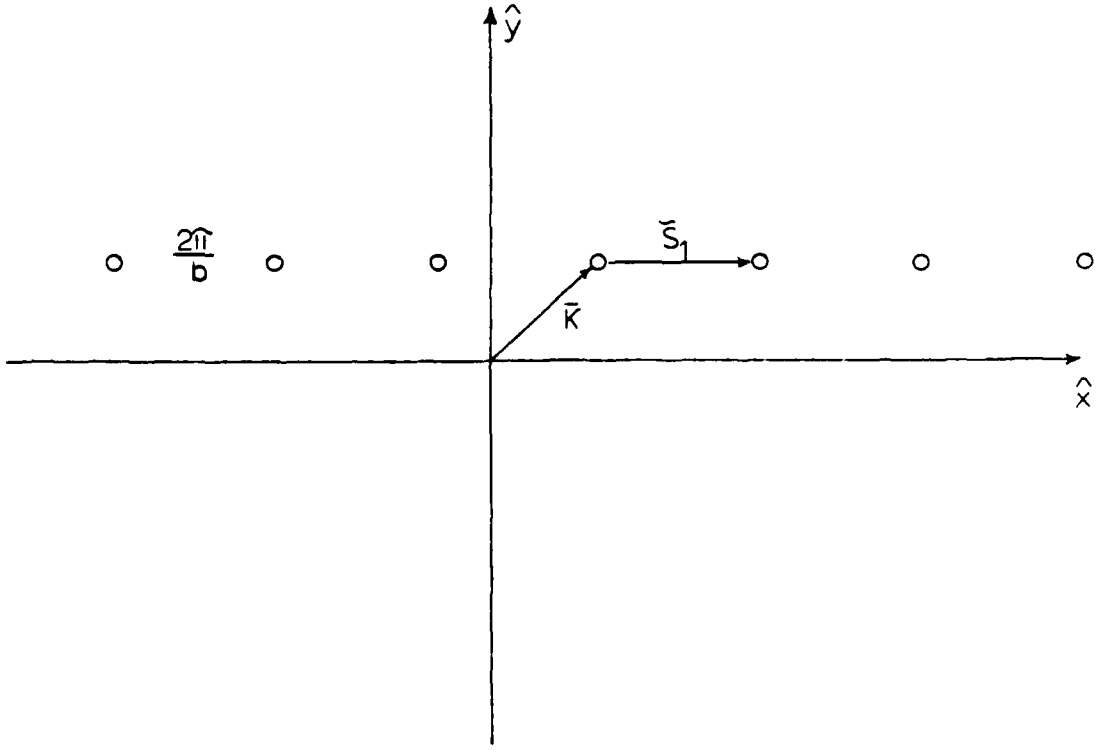

Figure 2.3 One-dimensional reciprocal lattice

single unit cell.

The periodic Green's function arises from Floquet's theorem which says, given a plane wave incident upon a periodic structure, all responses will have the same periodicity as the structure and a phase shift between unit cells which is the same as the phase shift of the incident plane wave. For example, the current in cell m is related to a corresponding position in cell 0 by

$$J(\vec{r}+mb\hat{x}) = J(\vec{r})e^{-j\vec{k}_{inc}\cdot mb\hat{x}} \tag{2.10}$$

It is not necessary, therefore, to consider the entire structure in a periodic geometry. Rather, a single unit cell may be considered along with a Green's function which reflects the relationship of Equation (2.10). The Green's function in this chapter is defined as the vector potential response at (x_0,y_0) due to an array of line sources located at (x',y') within each unit cell and having a cell-to- cell phase shift of $k_x b$ due to the incident plane wave as shown in Figure 2.4.

The response to an array of line sources may be obtained in two ways. In the spatial domain, an array of line sources located at x',y' in each unit cell may be represented as

$$J_a(x,y) = \sum_{m=-\infty}^{\infty} \delta(x-x'-mb)e^{-jk_x mb}\delta(y-y') \tag{2.11}$$

Summing the response at (x_0,y_0) due to each line source, the following expression is obtained:

$$G_p(x_0,y_0|x',y') = \frac{1}{4j}\sum_{m=-\infty}^{\infty} e^{-jk_x mb} H_0^2\left[k_0\sqrt{(x_0-x'-mb)^2+(y_0-y')^2}\right] \tag{2.12}$$

In the spectral domain, the Fourier transform pair is used to express the line array of Equation (2.11) as a series of current sheets. Each current sheet has a period dictated by the reciprocal lattice and a cell-to-cell phase shift dictated by the incident field (Equation (2.6)).

$$J_a(x,y) = \frac{1}{b}\sum_{m=-\infty}^{\infty} e^{+j\beta_{xm}(x-x')}\delta(y-y') \tag{2.13}$$

where

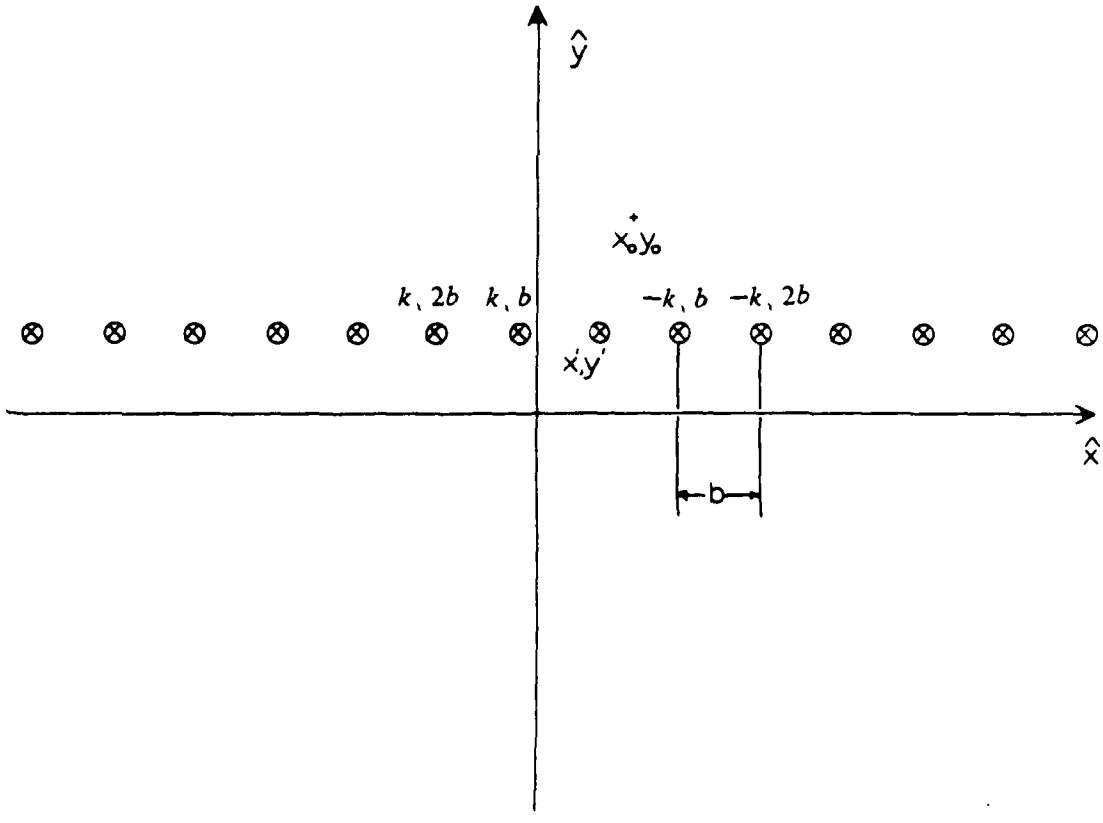

Figure 2.4 Array of line sources

$$\beta_{xm} = \frac{2\pi m}{b} - k_x$$

Adding the response at (x_0, y_0) due to each current sheet, the spectral domain Green's function is obtained

$$G_p(x_0, y_0 \mid x', y') = \frac{1}{b} \sum_{m=-\infty}^{\infty} \frac{e^{-j\beta_y |y_0 - y'|}}{2j\beta_y} e^{+j\beta_{xm}(x_0 - x')} \tag{2.14a}$$

where application of the radiation condition yields

$$\beta_y = \begin{cases} \sqrt{k_0^2 - \beta_{xm}^2} & \text{if } k_0^2 > \beta_{xm}^2 \\ -j\sqrt{\beta_{xm}^2 - k_0^2} & \text{if } \beta_{xm}^2 > k_0^2 \end{cases} \tag{2.14b}$$

To summarize, the solution of plane-wave scattering from periodic structures involves convolving the current in one unit cell with a periodic Green's function, which may be derived from two points of view. Working in the spatial domain, the response due to an array of line sources is found by summing the response due to each individual line source as shown in Equation (2.12). Alternatively, the spectral domain representation is obtained by representing the array of line sources as a series of current sheets and summing the response due to each current sheet as shown in Equation (2.14). The two representations of the Green's function are a Fourier transform pair sampled with a comb function. In the spatial domain, the sampling falls on the spatial lattice, while in the spectral domain, the sampling falls on the reciprocal lattice. This concept will be expanded further in Section 2.6.

2.4 Convergence Characteristics of G_p

In this section, the convergence characteristics of the periodic Green's function are examined in both the spatial domain (Equation (2.12)) and the spectral domain (Equation (2.14)). Using the asymptotic approximation for the Hankel function in Equation (2.12), the spatial domain summation is found to behave as

$$G_p(x_0, y_0 \mid x', y') \approx \sum_{m=-\infty}^{\infty} \frac{e^{-jk_x mb} e^{-jk_0\sqrt{(x_0 - x' - mb)^2 + (y_0 - y')^2}}}{\left|(x_0 - x' - mb)^2 + (y_0 - y')^2\right|^{\frac{1}{4}}} \tag{2.15}$$

for large values of m. This expression is convergent [6] only because of the phase variation in the numerator of the summand. For certain array spacings it doesn't converge at all and for all positions of the basis and testing functions, it converges slowly.

The spectral domain formulation of Equation (2.14a) converges rapidly as long as $y \neq y'$. In this report, this is called the "off plane" case since the observation point is located off the plane of the current sheet. The rapid convergence in the "off plane" case occurs because as m increases, the plane-wave response to the current sheets changes from propagating waves to evanescent waves as shown in Equation (2.14b) and the summand decays exponentially. For the "on plane" case ($y = y'$), the summand no longer has the exponential decay to aid convergence. It behaves as $e^{jm\Delta x}/m$ which converges slowly in most cases, and for some spacings of the basis and testing functions (i.e. $\Delta x = 0$), doesn't converge at all.

A further problem in the spectral formulation is that for certain combinations of array spacing, incidence angle and summation index (m), $\beta_y = 0$, which causes isolated terms of the summation to go to infinity. Since the function is sampled at discrete points, these singularities may be avoided by changing the angle of incidence slightly. The individual terms will all be finite, but the overall behavior of the function with respect to convergence will not change.

The reason that the different domains exhibit the convergence behavior outlined above can be traced to the existence of singularities in each of the domains. Recall that the periodic Green's functions are a Fourier transform pair sampled by the comb function in each domain. In the spectral domain (Equation 2.14a) the function is singular at the point where $\beta_y = 0$ which will inevitably occur for a continuous function representation. This implies that the Fourier transform (the spatial domain Green's function) is always a function with a wide support and is, therefore, slowly converging. Conversely, the spatial domain representation of the Green's function (Equation (2.12)) has a singularity when the argument of the Hankel function goes to zero. This singularity is inevitable for the continu-

ous function only when $y_0 = y'$ (on plane). For this case, the Fourier transform (the spectral domain Green's function) is of wide support and slowly convergent. As the $(y_0 - y')$ portion of the argument becomes larger, moving off plane, the continuous representation of the Hankel function becomes smoother and the convergence of the spectral term becomes more rapid.

To summarize, a pure spatial domain formulation doesn't converge well regardless of the position of the basis and testing functions. The pure spectral domain formulation involves a summation that converges well as long as the basis and testing functions are "off plane." Unfortunately, the "on plane" case inevitably occurs. For example, it occurs in the self term when the strips are rotated with respect to $\hat{x}$ ($\theta \neq 0^o$) or in all terms when the strips are flat ($\theta = 0^o$).

2.5 Smoothness of Basis/Test Functions to Help Convergence

The pure spatial formulation will be abandoned at this point due to its convergence problems that occur regardless of basis/test location. The pure spectral formulation, which has a convergence problem only in the "on plane" case, will be considered further. It is common, in the pure spectral formulation, to speed convergence in the "on plane" case by analytically performing the convolution operation using basis and testing functions [illegible] given combined degree of smoothness. To demonstrate this technique consider a TM to $\hat{z}$ plane wave incident on an array of flat strips ($\theta = 0^o$). The equation for an element of the Method of Moments' impedance matrix is

$$\begin{aligned} \langle \vec{T}, -\vec{E}^{scat} \rangle &= \int \vec{T}(x) \cdot \frac{j\omega\mu}{b} \int \vec{J}(x') \sum_{m=-\infty}^{\infty} \frac{e^{+j\beta_{xm}(x-x')}}{2j\beta_y} dx' dx \qquad (2.16) \\ &= \frac{j\omega\mu}{b} \sum_{m=-\infty}^{\infty} \frac{1}{2j\beta_y} \int T(x) e^{+j\beta_{xm}x} dx \int J(x') e^{-j\beta_{xm}x'} dx' \\ &= \frac{j\omega\mu}{b} \sum_{m=-\infty}^{\infty} \tilde{T}^*(\beta_{xm}) \tilde{J}(\beta_{xm}) \frac{1}{2j\beta_y} \end{aligned}$$

$\tilde{J}$ is the Fourier transform of the basis function in the $\hat{x}$ direction performed analytically.

$\tilde{T}^*$ is the complex conjugate of the Fourier transform of the test function also taken analytically. β_{xm} is defined in Equation (2.13). If the basis function is a pulse located at the origin, and the test function is a delta function located at x_T as shown in Figure 2.5, then

$$\tilde{J}(\beta_{xm}) = \Delta sinc\left(\frac{\beta_{xm}\Delta}{2}\right) \tag{2.17a}$$

and

$$\tilde{T}^*(\beta_{xm}) = e^{+j\beta_{xm}x_T} \tag{2.17b}$$

The summand now behaves as $1/m^2$ which converges regardless of spacing and quicker than the convergence of the Green's function alone.

Symbolically, the linearity of the Fourier transform has been used to change

$$T^R * J * F^{-1}\left[\tilde{G}\right] \tag{2.18}$$

to

$$F^{-1}\left[\tilde{T}^* \tilde{J}\, \tilde{G}\right] \tag{2.19}$$

In Equation (2.18), $T^R(x) = T(-x)$ is needed to get the testing function inner product into convolutional form. F^{-1} is the inverse Fourier transform and takes the form of a summation since β_{mx} is discrete.

The smoothness of the basis and testing functions becomes essential for convergence when differential operators arise in the integral equation, such as a TE to $\hat{z}$ plane wave incident on an array of flat strips ($\theta = 0^o$). In this case the left-hand side of the integral equation (Equation (2.9)) becomes

$$<\vec{T}, -\vec{E}^{scat}> = -\frac{1}{j\omega\epsilon b}\left[k_0^2 \int T(x)\int J(x')\sum_{m=-\infty}^{\infty}\frac{e^{+j\beta_{xm}(x-x')}}{2j\beta_y}dx'dx\right. \tag{2.20}$$

$$\left. + \frac{d}{dx}\int T(x)\int \frac{d}{dx'}J(x')\sum_{m=-\infty}^{\infty}\frac{e^{+j\beta_{xm}(x-x')}}{2j\beta_y}dx'dx\right]$$

In order to transfer the derivatives of the scalar potential term onto the basis and test functions, the functions must have a combined degree of smoothness of at least a triangular basis and a pulse test for the convolution integrals to make sense. The transfer of a

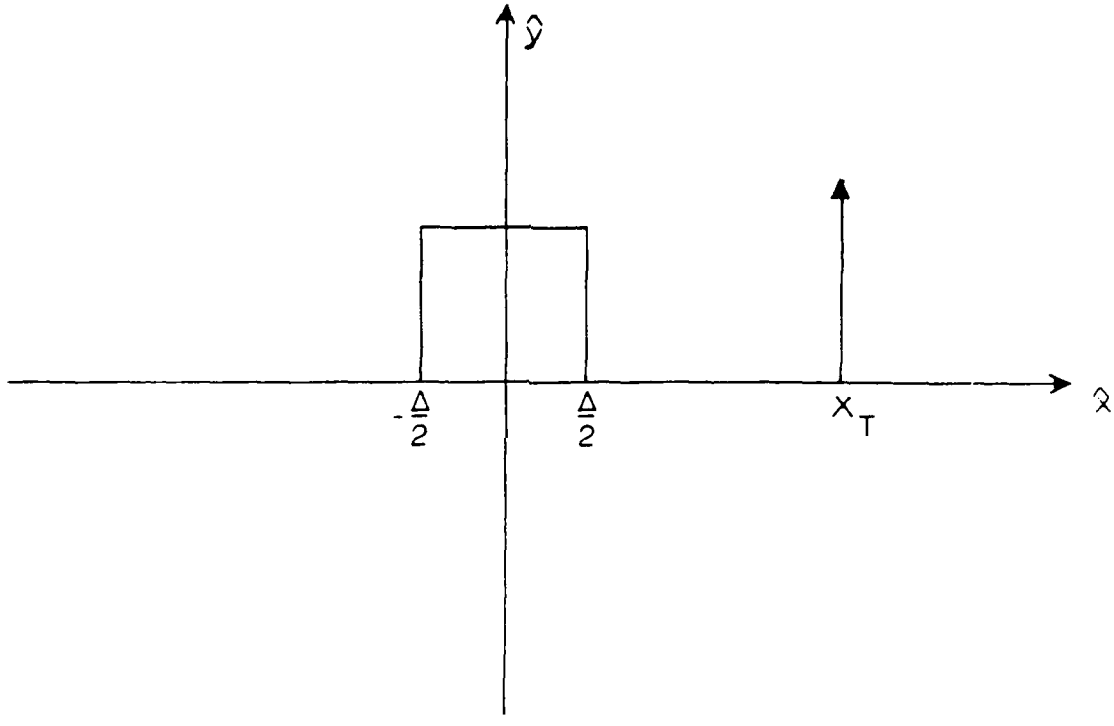

Figure 2.5 Basis and test functions for TM case

derivative onto the test function converts the pulse into a set of delta functions while the transfer of a derivative onto the basis function converts the triangle into a pulse doublet as shown in Figure 2.6. Performing the convolution of the basis, test and Green's functions analytically leads to the Fourier transform of a delta function, which behaves as 1, and the Fourier transform of the pulse doublet which behaves as $1/\beta_x$. These terms together with the $1/\beta_y$ behavior of the Green's function yield the same speed of convergence for the scalar potential term as that of the vector potential term for the TM case ($1/m^2$) discussed above. The TE vector potential term will converge much faster ($1/m^4$) since it has no derivatives and the functions to be convolved are, therefore, smoother.

If the derivatives are first transferred onto the Green's function in Equation (2.20), the following equation results:

$$-\frac{1}{j\omega\epsilon b}\int T(x)\int J(x')\sum_{m=-\infty}^{\infty}\frac{k_0^2-\beta_{xm}^2}{2j\beta_y}e^{+j\beta_{xm}(x-x')}dx'dx \tag{2.21}$$

The term arising from the vector potential term k_0^2 behaves similarly to the TM case and is slowly convergent. The term from the scalar potential (β_x^2) doesn't converge at all. In this case, the smoothness of the basis and testing functions is required to obtain convergence. Convolving analytically, Equation (2.21) becomes

$$-\frac{1}{j\omega\epsilon b}\sum_{m=-\infty}^{\infty}\frac{k_0^2-\beta_{xm}^2}{2j\beta_y}\tilde{T}^*(\beta_{xm})\tilde{J}(\beta_{xm}) \tag{2.22}$$

The level of smoothness needed for the above sum to be convergent is at least that exhibited by triangular basis and pulse test functions. This is the same level of smoothness needed when the derivatives were transferred to the basis and testing functions.

In summary, for flat strips ($\theta = 0^o$), the derivatives may be transferred onto the Green's function, and the smoothness of the basis and testing functions may be used to help convergence, or the derivatives may be transferred onto the basis and testing functions explicitly and then the convolution may be performed. In either case, the speed of convergence and the level of smoothness required are the same and the order of the operations

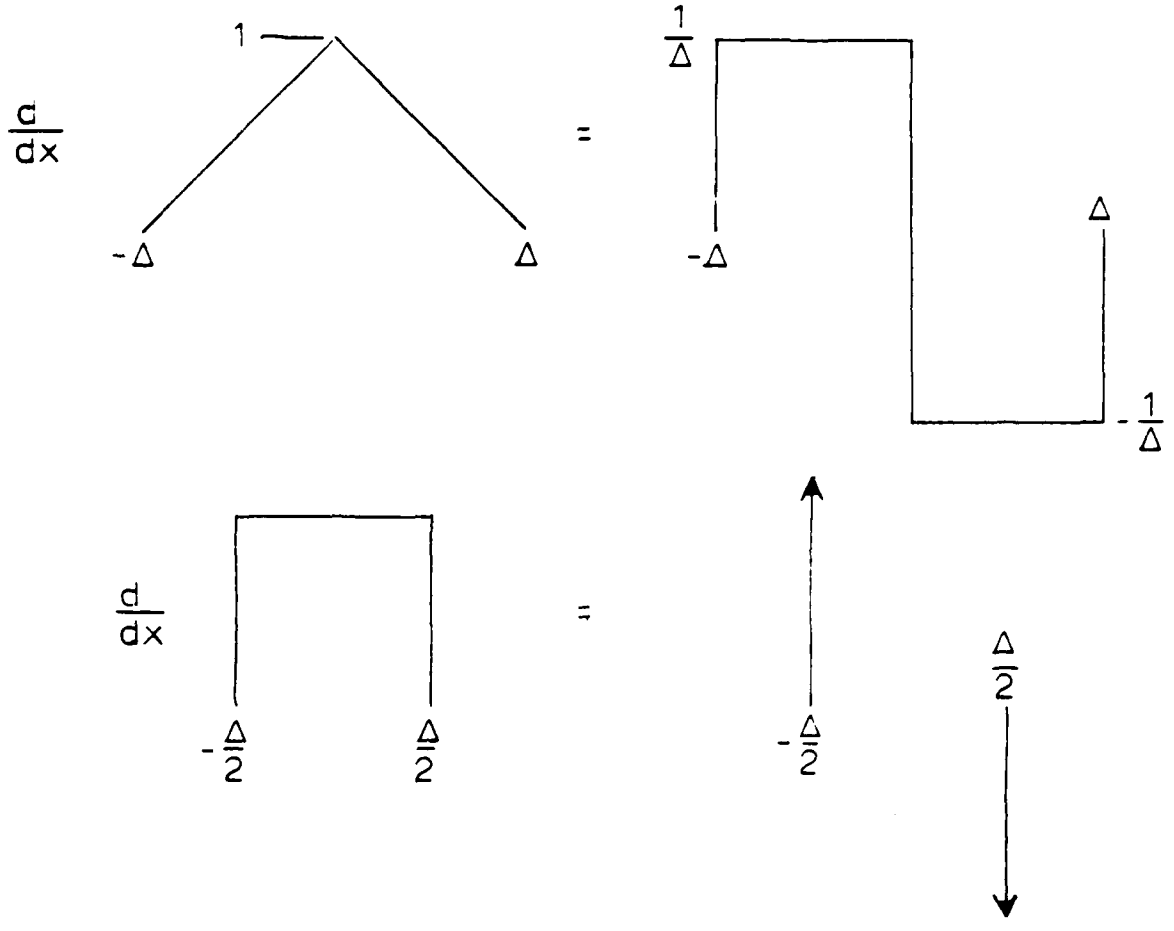

Figure 2.6 Transfer of scalar potential derivatives onto the basis and test functions

does not matter.

In contrast to the flat case, when the strips are rotated ($\theta \neq 0^{o}$) with respect to the $\hat{x}$ axis, the order of operations does matter. If the derivatives are first transferred to the Green's function, the resulting sum will not converge regardless of the level of smoothness in the basis and test functions. This is best illustrated by examining the case in which the strips are rotated 90 degrees to the $\hat{x}$ axis. With the derivatives transferred to the Green's function, the expression for the the matrix elements becomes

$$<T,-E^{scat}> = -\frac{1}{j\omega\epsilon b}\sum_{m=-\infty}^{\infty}\int_{y}\int_{y'}\tilde{J}(\beta_{xm},y')\tilde{T}^{*}(\beta_{xm},y)\frac{e^{-j\beta_{y}|y-y'|}}{2j\beta_{y}}(k_{0}^{2}-\beta_{y}^{2})dy'dy \qquad (2.23)$$

If J is a triangular function along the strip and T is a pulse function, which led to convergent terms in the flat case, then for no overlap between the basis and test functions (see Figure 2.7) Equation (2.23) becomes

$$-\frac{1}{j\omega\epsilon b}\sum_{m=-\infty}^{\infty}\Delta sinc^{2}\left|\frac{\beta\Delta}{2}\right|\Delta sinc\left|\frac{\beta\Delta}{2}\right|e^{-j\beta_{y}y_{T}}\frac{(k_{0}^{2}-\beta_{y}^{2})}{2j\beta_{y}} \qquad (2.24)$$

Note that the convergence problem arising from the scalar potential term (β_{y}^{2}) is mitigated by the smoothness of the basis and testing functions and the summand behaves as $1/m^{2}$ exactly like the flat case. Also note that since this is an "off plane" case, the exponential decay is the dominant behavior of the summand.

When there is complete overlap between basis and testing functions as shown in Figure 2.8, Equation (2.23) becomes

$$-\frac{1}{j\omega\epsilon b}\sum_{m=-\infty}^{\infty}\frac{(k_{0}^{2}-\beta_{y}^{2})}{2j\beta_{y}}\left\{\left|\frac{3\Delta}{2j\beta_{y}}+\frac{2e^{-j\beta_{y}\Delta}}{j\beta_{y}^{3}\Delta}\right|\left|1-e^{+j\frac{\beta_{y}\Delta}{2}}\right|\right. \qquad (2.25)$$

$$\left.+\left|\frac{4}{j\beta_{y}^{3}\Delta}-\frac{2e^{-j\beta_{y}\Delta}}{j\beta_{y}^{3}\Delta}\right|\left|1-e^{-j\frac{\beta_{y}\Delta}{2}}\right|\right\}$$

The second and third groups of terms in the braces have the $1/\beta_{y}^{3}$ behavior dictated by the level of basis/testing smoothness chosen. Additionally, since these terms represent the

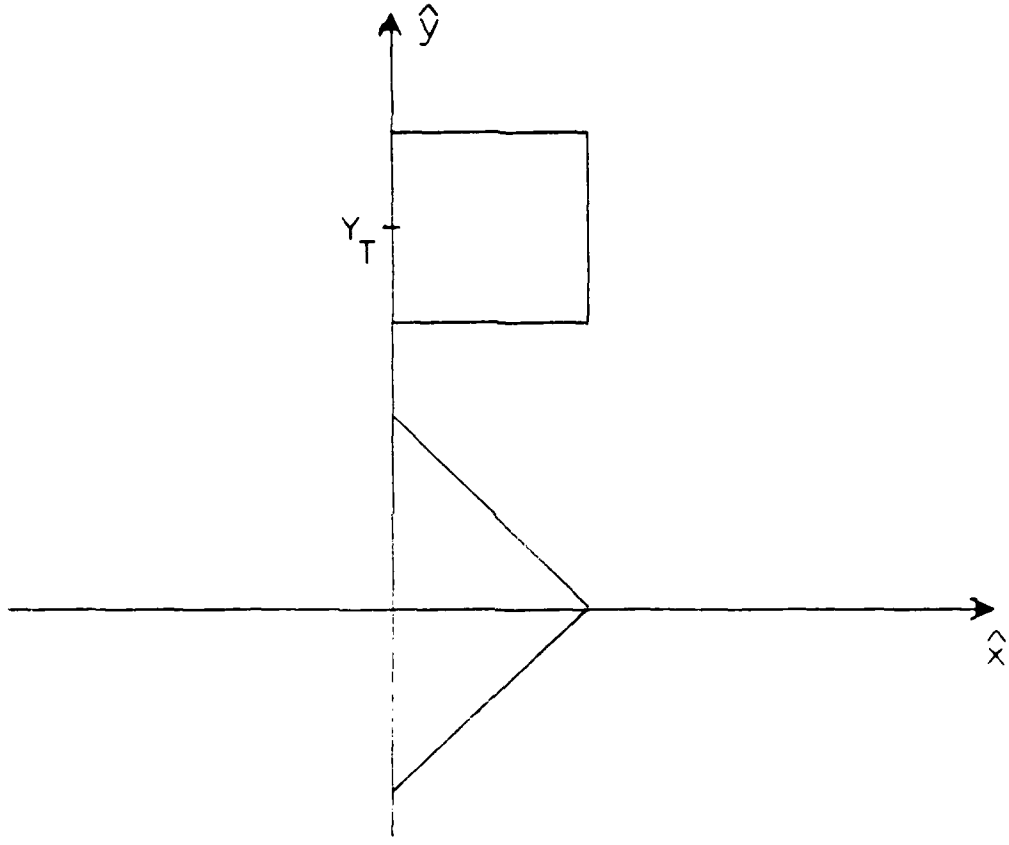

Figure 2.7 No overlap between basis and test functions

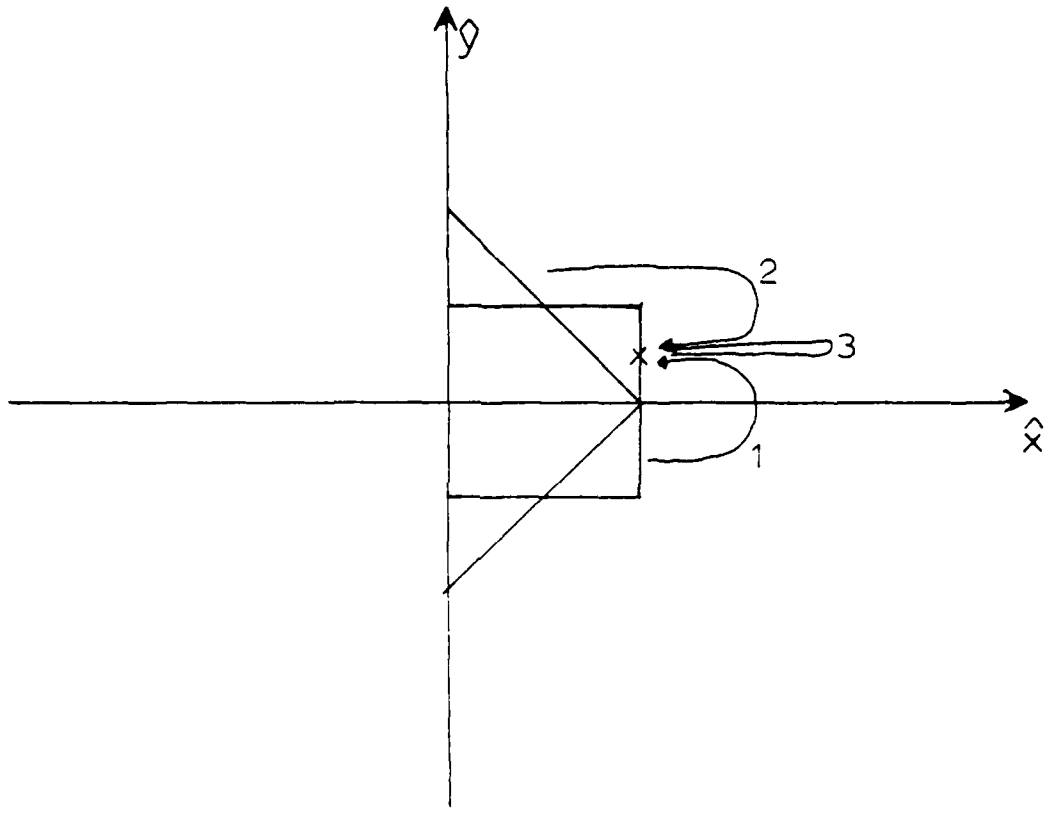

Figure 2.8 Complete overlap between basis and test functions

contribution of the basis to the parts of the test not on the same plane (labeled 1 and 2 in Figure 2.8), there is an exponential decay in these terms which also aids convergence. The first term in the braces does not converge. It represents contributions of the basis functions to portions of the test function in the same plane (labeled 3 in Figure 2.8). Consequently, the first term has no exponential decay. Additionally, it has only a $1/\beta_y$ behavior rather than the $1/\beta_y^3$ behavior expected from the level of smoothness under consideration.

In order to understand this problem, the expression

$$\int \tilde{T}(\beta_{xm}, y) \int \tilde{J}(\beta_{xm}, y') e^{-j\beta_y |y-y'|} dy' dy \tag{2.26}$$

will be examined for basis and testing functions with various degrees of smoothness, but not necessarily the sufficient degree of smoothness needed to solve the TE case under consideration. For pulse basis and delta testing functions with no overlap, Equation (2.26) becomes

$$\Delta sinc\left(\frac{\beta_y \Delta}{2}\right) e^{-j\beta_y y_T} \tag{2.27}$$

Equation (2.27) behaves as $1/\beta_y$ as expected from a pulse/delta degree of smoothness. The exponential decay arises from the basis and test being "off plane" from one another. With complete overlap, the expression becomes

$$\frac{2}{j\beta_y} + \frac{2}{j\beta_y} e^{-j\frac{\beta_y \Delta}{2}} \tag{2.28}$$

The second term represents the "off plane" contributions of the basis to the test. It has a $1/\beta_y$ dependence which stems from the smoothness of the basis and testing functions and an exponential decay which stems from the "off plane" nature of the contributions. The first term represents the single "on plane" contribution from the point y=0 on the basis. This term also has a $1/\beta_y$ dependency which does not arise from the smoothness of the basis and testing function. The important thing to note is that the first term in Equation (2.28) has the same dependency as the first term in the triangle/pulse case (Equation (2.25)) even though the triangle/pulse case has a higher degree of smoothness than the

pulse/delta case.

For pulse basis and pulse testing without overlap, Equation (2.26) becomes

$$\Delta^2 sinc^2\left(\frac{\beta_y \Delta}{2}\right) e^{-j\beta_y y_T} \tag{2.29}$$

This expression has a $1/\beta_y^2$ dependency related to the basis/test smoothness exactly as was found in the flat case. The exponential decay arises from the "off plane" nature of the problem. For complete overlap the expression becomes

$$\frac{2\Delta}{j\beta_y} - \frac{4}{j\beta_y^2}\sin\left(\frac{\beta_y \Delta}{2}\right) e^{-j\frac{\beta_y \Delta}{2}} \tag{2.30}$$

Again the second term has the expected $1/\beta_y^2$ decay from the smoothness and the exponential decay from "off plane" contributions. The first term has a $1/\beta_y$ decay which is the same as the "on plane" terms of the previous cases.

The pattern that emerges is as follows: when there is no overlap between basis and testing functions, both exponential decay and degree of smoothness contribute to rapid convergence. In this case the derivatives may be transferred to the Green's function. For the case in which there is overlap between the basis and test functions (even touching at one point), one term arises which behaves as $1/\beta_y$ regardless of the smoothness of the basis and testing functions. This term represents the "on plane" contribution of the basis to the testing function and, therefore, has no exponential decay. For this case, the derivatives may not be transferred to the Green's function to obtain a convergent summation. Rather, basis and testing functions must be chosen with a level of smoothness to accept the derivatives, and the derivatives must be explicitly transferred onto the basis and testing functions.

To ensure that the above problem is not unique to the $\theta = 90^\circ$ case, a strip of arbitrary rotation θ will be examined for completely overlapping pulse basis and pulse test functions. For this case, the "on plane" contribution of Equation (2.26) becomes

$$\left| \frac{\Delta}{j(\beta_x \cos\theta + \beta_y \sin\theta)} - \frac{\Delta}{j(\beta_x \cos\theta - \beta_y \sin\theta)} \right| \tag{2.31}$$

When $\theta = 0^o$ (the flat case), the terms in the braces cancel, but for all other cases, the terms in the braces remain, leading to nonconvergence of the sum.

To summarize, in the flat case, all derivatives may be transferred onto the Green's function, and the smoothness of the basis and testing functions ensures the convergence of the sum. The degree of smoothness required of the basis and testing functions is the same, whether the derivatives are transferred onto the basis and testing functions or onto the Green's function. A higher degree of smoothness leads to faster convergence in the sum. In contrast, in the rotated strip case, the derivatives must be transferred onto the basis and testing functions explicitly before convolving. To transfer the derivatives onto the Green's function leads to nonconvergent terms representing "on plane" contributions of the basis to the test function. Increasing the degree of smoothness has absolutely no effect on the speed of convergence. *Pulse/delta, pulse/pulse and triangle/pulse* all have $1/\beta_y$ terms. Note that this is sufficient for convergence as long as there are no β terms in the numerator representing derivatives transferred to the Green's function.

2.6 Acceleration of Convergence

A result of Section 2.5 showed that it is necessary to transfer all derivatives in the scalar potential term to the basis and testing functions when computing the matrix elements for a strip grating of arbitrary rotation. This operation reduces triangular basis and pulse testing functions to combinations of pulse basis and delta testing functions if both basis and test take a derivative (Figure 2.6). In this report, the vector potential term calculation will be simplified by approximating the triangular basis by a pulse with the same moment and approximating the pulse test by a delta function weighted by the pulse support [12] (see Figure 2.9). This approximation can be justified by observing that when the test function is near the basis function, the scalar potential term is the dominant contribu-

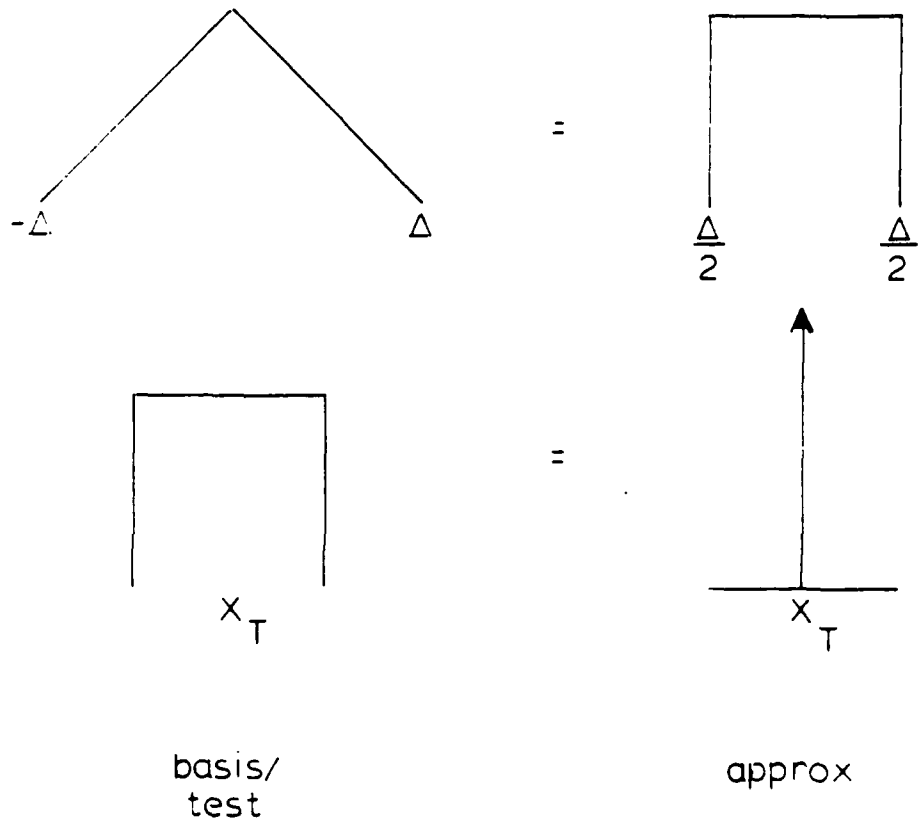

Figure 2.9 Approximations used for the basis and test functions in the vector potential terms

tor to the matrix element and the value of the vector potential term is unimportant. As the distance between basis and testing functions is increased, making the vector potential more important, the moment of the current is the quantity that determines the value of the vector potential. The moments are the same for the triangle basis and the approximate pulse basis. Through the above approximations, all of the integrals are reduced to the same form: one of finding the response at the test location x_T, y_T to an array of current pulses of arbitrary rotation as shown in Figure 2.10.

In order to accelerate the convergence of the summation, the Poisson summation formula will be used. This method makes use of the fact that a smooth, nonsingular function with a wide support in one domain (either spatial or spectral) has a narrow support in the other domain. It also employs Parseval's theorem

$$\int h(x) f(x) dx = \frac{1}{2\pi} \int \tilde{H}(\beta) \tilde{F}(\beta) d\beta \tag{2.32}$$

If h(x) is chosen to be a comb function whose elements fall on the spatial lattice

$$h(x) = \sum_{m=-\infty}^{\infty} e^{-jk_s mb} \delta(x - mb) \tag{2.33a}$$

then its Fourier transform $\tilde{H}(\beta)$ is also a comb function whose elements fall on the reciprocal lattice.

$$\tilde{H}(\beta) = \frac{1}{b} \sum_{m=-\infty}^{\infty} \delta\left|\beta - \left|\frac{2\pi m}{b} - k_s\right|\right| \tag{2.33b}$$

Thus, using Parseval's theorem, a series may be represented in either domain by

$$\sum_{m=-\infty}^{\infty} e^{-jk_s mb} f(mb) = \int \sum_{m=-\infty}^{\infty} e^{-jk_s mb} \delta(x - mb) f(x) dx \tag{2.34}$$

$$= \frac{1}{b} \int \sum_{m=-\infty}^{\infty} \delta\left|\beta - \left|\frac{2\pi m}{b} - k_s\right|\right| \tilde{F}(\beta) d\beta$$

$$= \sum_{m=-\infty}^{\infty} \tilde{F}\left|\frac{2\pi m}{b} - k_s\right|$$

If f(x) has a wide support and is nonsingular, implying slow convergence, then $\tilde{F}(\beta)$ will

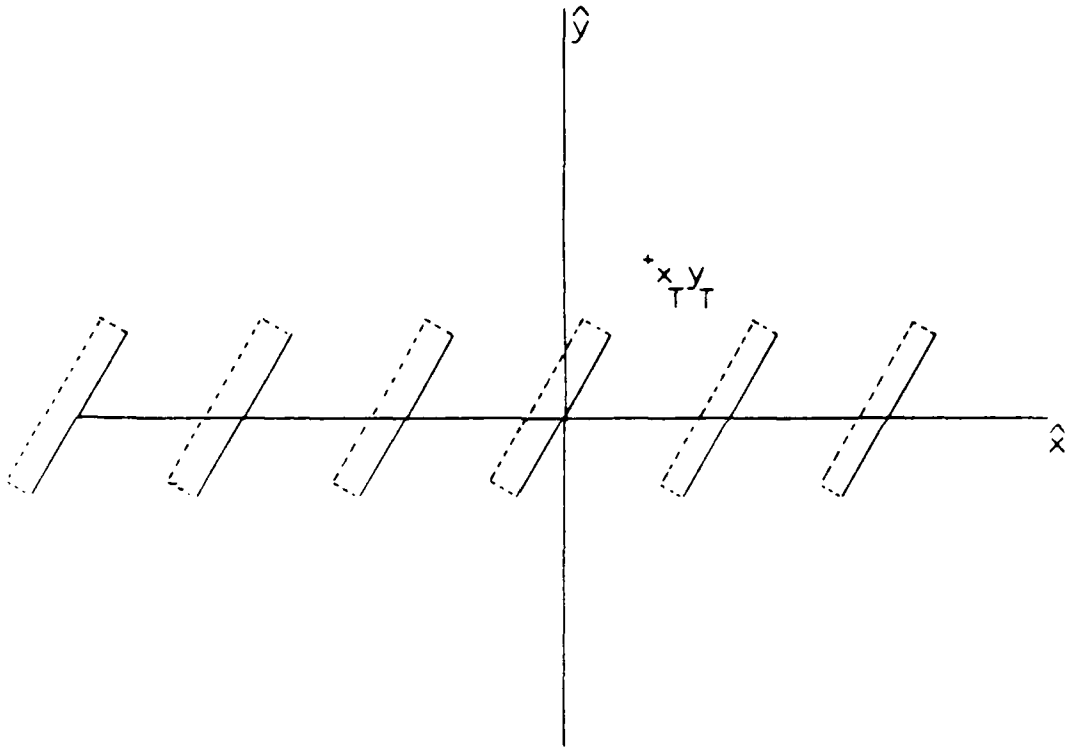

Figure 2.10 Array of current pulses tested at a point

have a narrow support, implying rapid convergence and vice versa.

To demonstrate a fundamental problem with this approach, Equation (2.34) is applied to the slowly convergent "on plane" case of the pure spectral domain (Equation (2.14a)).

$$\frac{1}{b}\sum_{m=-\infty}^{\infty}\frac{1}{2j}\frac{e^{-j\left|\frac{2\pi m}{b}-k_x\right|(z-z')}}{\left|k_0^2-\left(\frac{2\pi m}{b}-k_x\right)^2\right|^{\frac{1}{2}}}=\frac{1}{b}\int\sum_{m=-\infty}^{\infty}\delta\left|\beta-\left|\frac{2\pi m}{b}-k_x\right|\right|\frac{1}{2j}\frac{e^{+j\beta(z-z')}}{\sqrt{k_0^2-\beta^2}} \quad (2.35)$$

In terms of Parseval's theorem,

$$\tilde{F}(\beta)=\frac{e^{+j\beta(z-z')}}{2j\sqrt{k_0^2-\beta^2}} \quad (2.36a)$$

$$f(x)=\frac{1}{2\pi}\int\frac{e^{+j\beta(z_0-z')}}{2j\sqrt{k_0^2-\beta^2}}e^{+j\beta x}\,d\beta \quad (2.36b)$$

As discussed previously, the summand in Equation (2.35) is singular when $\beta_{xm}^2=k_0^2$, but since β_{xm} is discrete in m the singularity is avoidable. In Equation (2.36b), however, β is continuous and the singularity cannot be avoided. The integrand is sharply peaked, so it is expected that application of Poisson acceleration will not help convergence. In spite of this, if the integration in Equation (2.36b) is performed,

$$f(x)=\frac{1}{4j}H_0^2(k_0|x_0-x'-x|) \quad (2.37)$$

is obtained. Applying Parseval's theorem yields

$$\frac{1}{2\pi}\int f(x)h(x)dx=\frac{1}{4j}\sum_{m=-\infty}^{\infty}e^{-jk_x mb}H_0^2(k_0|x_0-x'-mb|) \quad (2.38)$$

This is the pure spatial formulation of the periodic Green's function which is slowly convergent. If the Poisson summation formula is applied to Equation (2.38), the result is the pure spectral domain formulation of the Green's function "on plane." The unavoidable singularity of the Hankel function as the argument approaches zero leads to the slow convergence of the "on plane" sum in the pure spectral domain.

In both spectral and spatial domains, application of the Poisson summation formula did not speed convergence because it was applied to a peaked function with an unavoidable

singularity. Thus, a better strategy is to subtract from the singular function an auxiliary, nonsingular function that is asymptotically equal to the singular function for large m; then add the nonsingular asymptotic function back in. The Poisson summation formula may be successfully applied to this smooth, wide, asymptotic function. First, working with the spectral domain:

$$\sum_{m=-\infty}^{\infty} \frac{1}{2j} \frac{e^{+j\beta_{xm}(x_0-x')}}{\sqrt{k_0^2-\beta_{xm}^2}} = \tag{2.39}$$

$$\sum_{m=-\infty}^{\infty} \frac{e^{+j\beta_{xm}(x_0-x')}}{2j} \left| \frac{1}{\sqrt{k_0^2-\beta_{xm}^2}} - \frac{1}{-j\sqrt{u^2+\beta_{xm}^2}} \right|$$

$$+ \sum_{m=-\infty}^{\infty} \frac{1}{2} \frac{e^{+j\beta_{xm}(x_0-x')}}{\sqrt{u^2+\beta_{xm}^2}}$$

The first summation is done in the spectral domain and converges as $1/\beta_{xm}^2$. The second summation is never singular so the Poisson summation formula can be successfully applied. The second sum becomes

$$\sum_{m=-\infty}^{\infty} e^{-jk_x mb} K_0(u\,|x_0-x'-mb\,|) \tag{2.40}$$

where K_0 is the modified Bessel function which exponentially decreases with increasing argument.

The operations of Equation (2.18) may be rewritten using Equation (2.39) as

$$T^R * J * F^{-1}(G) = T^R * J * \left| F^{-1}(\tilde{G}-\tilde{G}^a) + G^a \right| \tag{2.41}$$

The inverse Fourier transform F^{-1} is a summation. The smooth auxiliary function, $\tilde{G}^a$, has the same asymptotic behavior as the desired function $\tilde{G}$ and is summed in the spatial domain through use of the Poisson summation formula. In Equation (2.41), the operations in brackets may be viewed as a way to accelerate a slowly convergent summation by breaking it up into two rapidly convergent summations.

The convolution operation of Equation (2.41) may be distributed onto each domain and performed analytically in the spectral domain, according to

$$F^{-1}\left[\tilde{T}\cdot\tilde{J}\ (\tilde{G}-\tilde{G}^{a})\right]+T^{R}*J*G^{a} \tag{2.42}$$

This is equivalent to computing the impedance matrix elements by adding the elements of two matrices: one computed in the spectral domain and the other computed in the spatial domain.

To accelerate the spatial domain summation successfully for the "on plane" case $(y_0-y'=0)$ the asymptotic behavior of the Hankel function must be removed by moving the observation point of the auxiliary term off the plane, cb units.

$$\frac{1}{4j}\sum_{m=-\infty}^{\infty}e^{-jk_x mb}H_0^2\left[k_0\sqrt{(x_0-x'-mb)^2}\right]= \tag{2.43}$$

$$\frac{1}{4j}\sum_{m=-\infty}^{\infty}e^{-jk_x mb}\left[H_0^2\left[k_0\sqrt{(x_0-x'-mb)^2}\right]-H_0^2\left[k_0\sqrt{(x_0-x'-mb)^2+cb^2}\right]\right]$$

$$+\frac{1}{4j}\sum_{m=-\infty}^{\infty}e^{-jk_x mb}H_0^2\left[k_0\sqrt{(x_0-x'-mb)^2+cb^2}\right]$$

The first summation remains in the spatial domain and converges rapidly because its asymptotic behavior is being subtracted out. The second summation is brought into the spectral domain using the Poisson summation formula. To apply Parseval's theorem to the second sum, the following equations are needed:

$$f(x)=\frac{1}{4j}H_0^2\left[k_0\sqrt{(x_0-x'-X)^2+cb^2}\right] \tag{2.44a}$$

$$\tilde{F}(\beta)=\int\frac{1}{4j}H_0^2\left[k_0\sqrt{X^2+cb^2}\right]e^{-j\beta X}dX\ e^{+j\beta(x_0-x')} \tag{2.44b}$$

Application of Parseval's theorem yields

$$\frac{1}{2\pi}\int\tilde{F}(\beta)\tilde{H}(\beta)d\beta=\frac{1}{b}\sum_{m=-\infty}^{\infty}\frac{e^{-jcb\beta_y}}{2j\beta_y}e^{+j\beta_{xm}(x_0-x')} \tag{2.45}$$

where

$$\beta_{xm}=\frac{2\pi m}{b}-k_x$$

$$\beta_y=\begin{cases}\sqrt{k_0^2-\beta_{xm}^2} & \text{if } k_0^2>\beta_{xm}^2\\ -j\sqrt{\beta_{xm}^2-k_0^2} & \text{if } \beta_{xm}^2>k_0^2\end{cases}$$

Since this is in the spectral domain for an "off plane" observation point, this sum is rapidly

convergent.

As in the acceleration of the spectral domain formulation, the above procedure may be treated as a way of quickly summing the spatial periodic Green's function,

$$T^R * J * G = T^R * J * \left[(G - G^a) + F^{-1}(\tilde{G}^a)\right] \tag{2.46}$$

By distributing the convolution operation of Equation (2.46) onto the different domains and performing the convolutions analytically in the spectral domain, the following is obtained.

$$T^R * J * (G - G^a) + F^{-1}(\tilde{T}\,\tilde{J}\,\tilde{G}^a) \tag{2.47}$$

If cb is allowed to equal zero, the asymptotic testing point is moved "on plane." The first term goes to zero, and the Green's function is summed entirely in the spectral domain. Since the test point of the asymptotic term is now "on plane," the summation is the slowly convergent pure spectral domain approach. The next section will discuss the details of implementing Equations (2.46) and (2.47).

2.7 Numerical Implementation of the Spatial Domain Acceleration

In this section, the details of implementing the spatial domain acceleration procedure will be examined. The accelerated periodic Green's function, shown in Equation (2.43) with $y_0 - y' \neq 0$, is expressed as a weighted combination of the spatial domain and spectral domain.

$$G_p(x_0, y_0 \mid x', y') = \frac{1}{4j} \sum_{m=-\infty}^{\infty} e^{-jk_x mb} \tag{2.48}$$

$$\left[H_0^2\left(k_0\sqrt{(x_0 - x' - mb)^2 + (y_0 - y')^2}\right) - H_0^2\left(k_0\sqrt{(x_0 - x' - mb)^2 + (|y_0 - y'| + cb)^2}\right)\right]$$

$$+ \frac{1}{b} \sum_{m=-\infty}^{\infty} \frac{e^{-j(|y_0 - y'| + cb)\beta_y}}{2j\beta_y} e^{j\beta_{xm}(x_0 - x')}$$

The factor that determines the weighting given to each domain is c, which is a measure of how far "off plane" the testing point of the asymptotic term in the Green's function is located.

Figures 2.11-2.14 show the nature of the real part of the summand versus term number (m) for various c's. In this report, c is always multiplied by the cell size (b), for example, c=0.1 and cell size = 0.7m moves the test point of the asymptotic Green's function (cb) 0.07 m "off plane." In Figure 2.11, c=0.001 so the terms of the spatial summation are small in magnitude and highly peaked around the m=0 term. The spectral domain has a much larger magnitude which oscillates around zero to term 20 and beyond. For this value of c, the spectral domain makes most of the contribution to the overall sum and converges slowly. As c is increased, moving further "off plane" (c=0.01 and 0.1), the spatial domain becomes larger in magnitude and loses its peaked nature. The spectral domain, on the other hand, becomes smaller in magnitude and more peaked around m=0. In Figure 2.13, for example, when c=0.1, the spatial term magnitude is oscillating around zero until outside the m=-16:16 core while the spectral magnitude is zero outside the m=-4:4 core. When c=1, as shown in Figure 2.14, the spectral domain terms are essentially zero and all the weight is on the spatial domain which, like the spectral domain of Figure 2.11, oscillates around zero to term 20 and beyond.

The shifting of weight from the spectral domain to the spatial domain as c moves "off plane" is also seen in Figures 2.15-2.18. In this set of figures, the value of the sum in each domain is observed as the limits of the summation are increased from m=-1:1 to m=-100:100. For c=0.001, the spectral domain carries all the weight and oscillates about its true value past the sum limit of m=100. As the asymptotic observation point is moved further "off plane" (c=0.01,0.05 and 0.1), the spectral domain sum converges in a fewer number of terms and becomes smaller while the spatial domain sum requires more terms to converge and makes a larger contribution.

The question that arises is: Can the parameter c be chosen to minimize the time needed to do the two summations in the spatial and spectral domains? In order to answer this question, a parameter study was performed where the sum limit needed for conver-

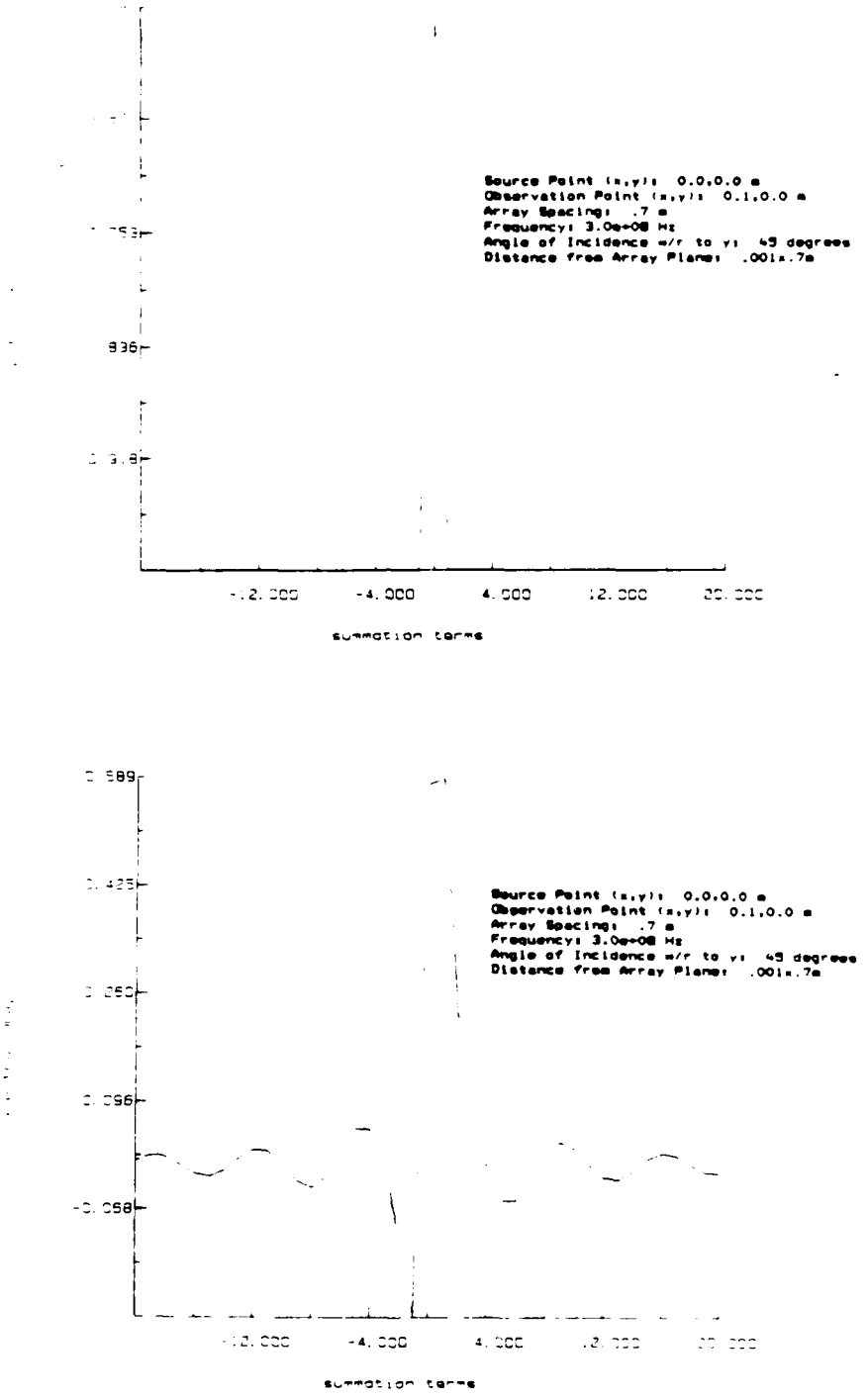

Figure 2.11 Spatial and spectral summand vs. term number for ϵ=0.001

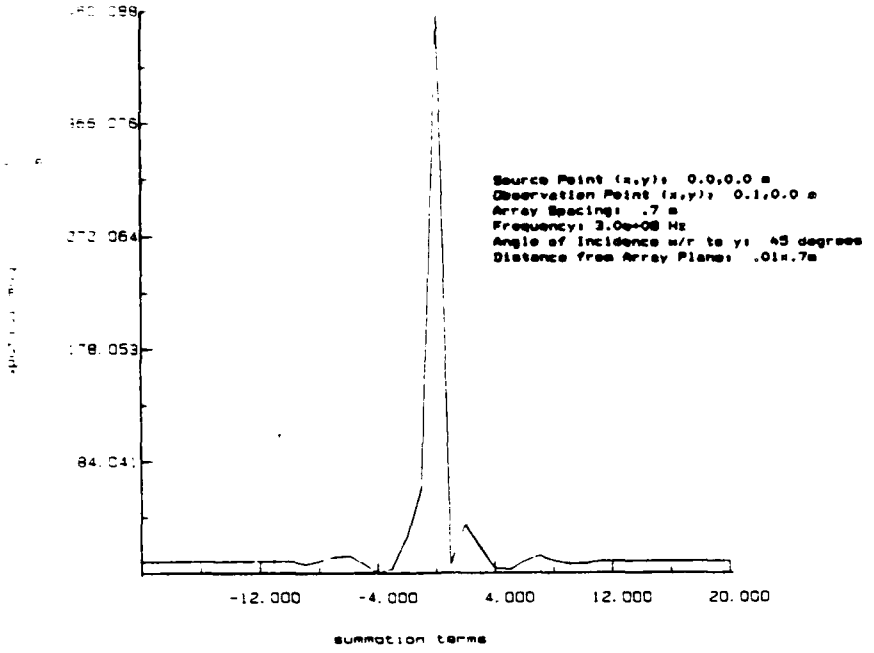

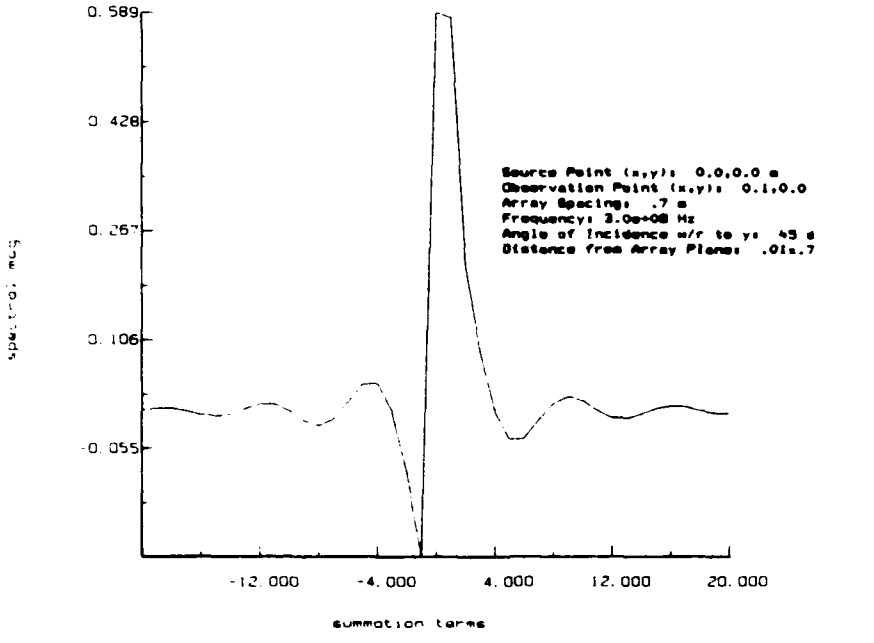

Figure 2.12 Spatial and spectral summand vs. term number for c=0.01

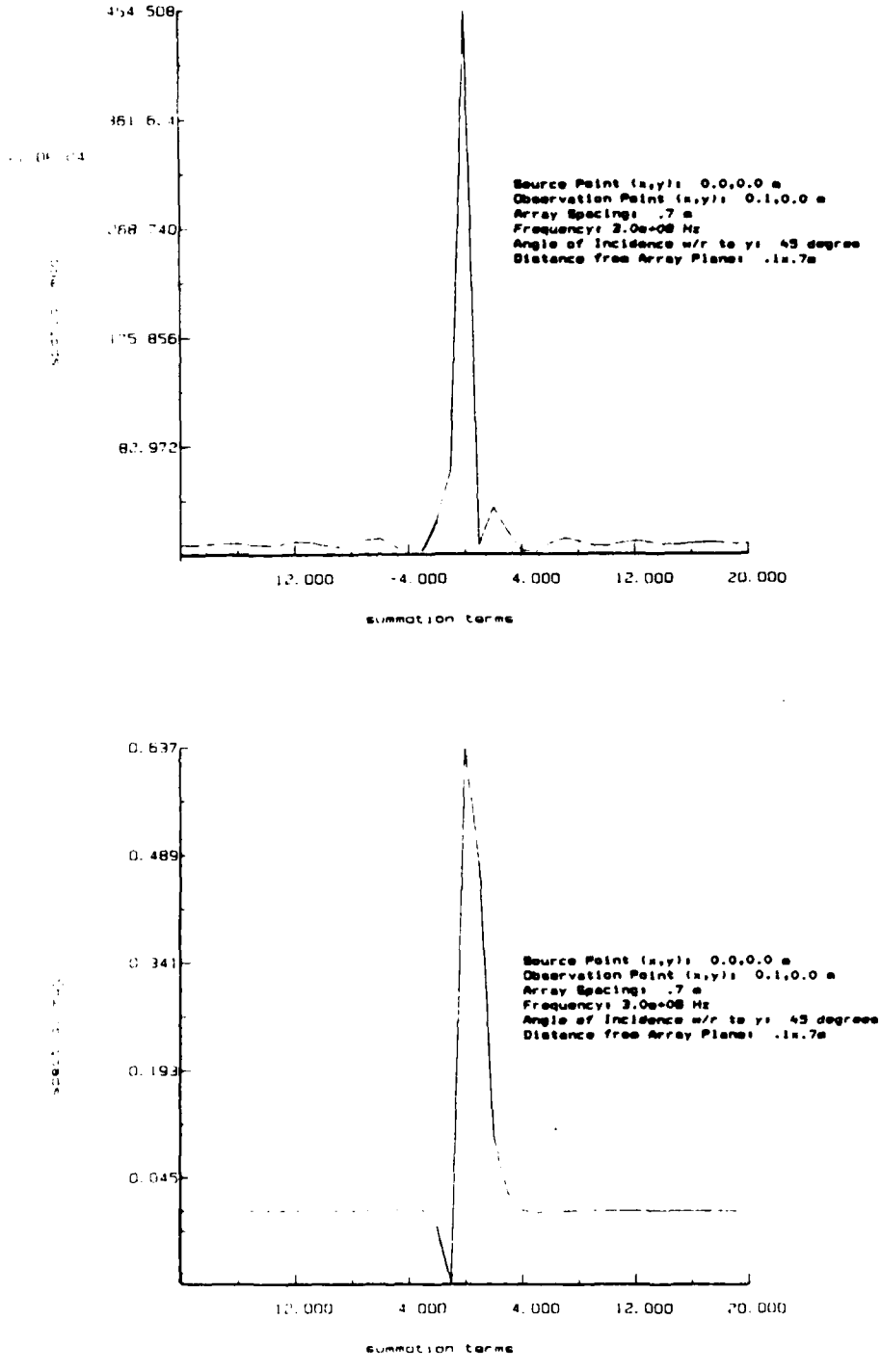

Figure 2.13 Spatial and spectral summand vs. term number for c=0.1

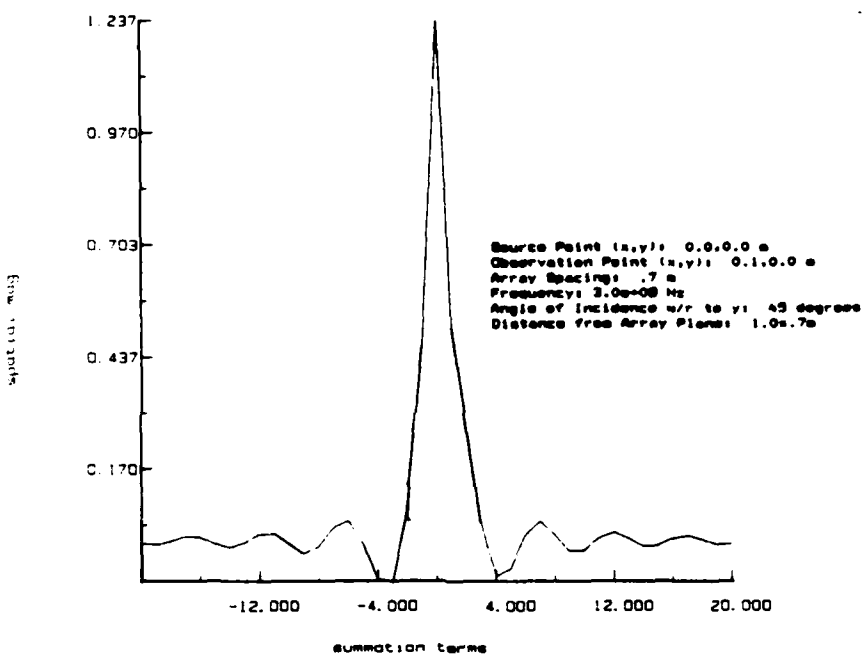

Figure 2.14 Spatial and spectral summand vs. term number for c=1.0

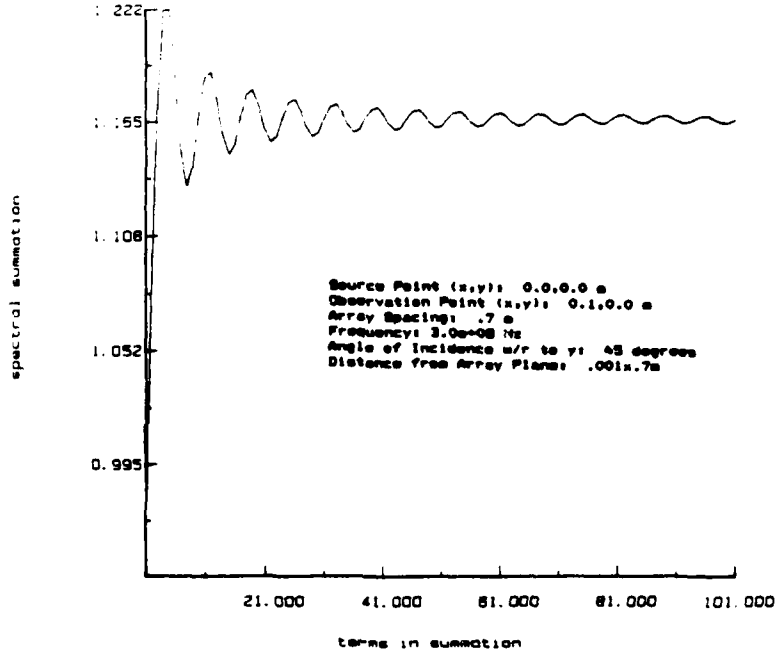

Figure 2.15 Spectral and spatial sum vs. sum limit for c=0.001

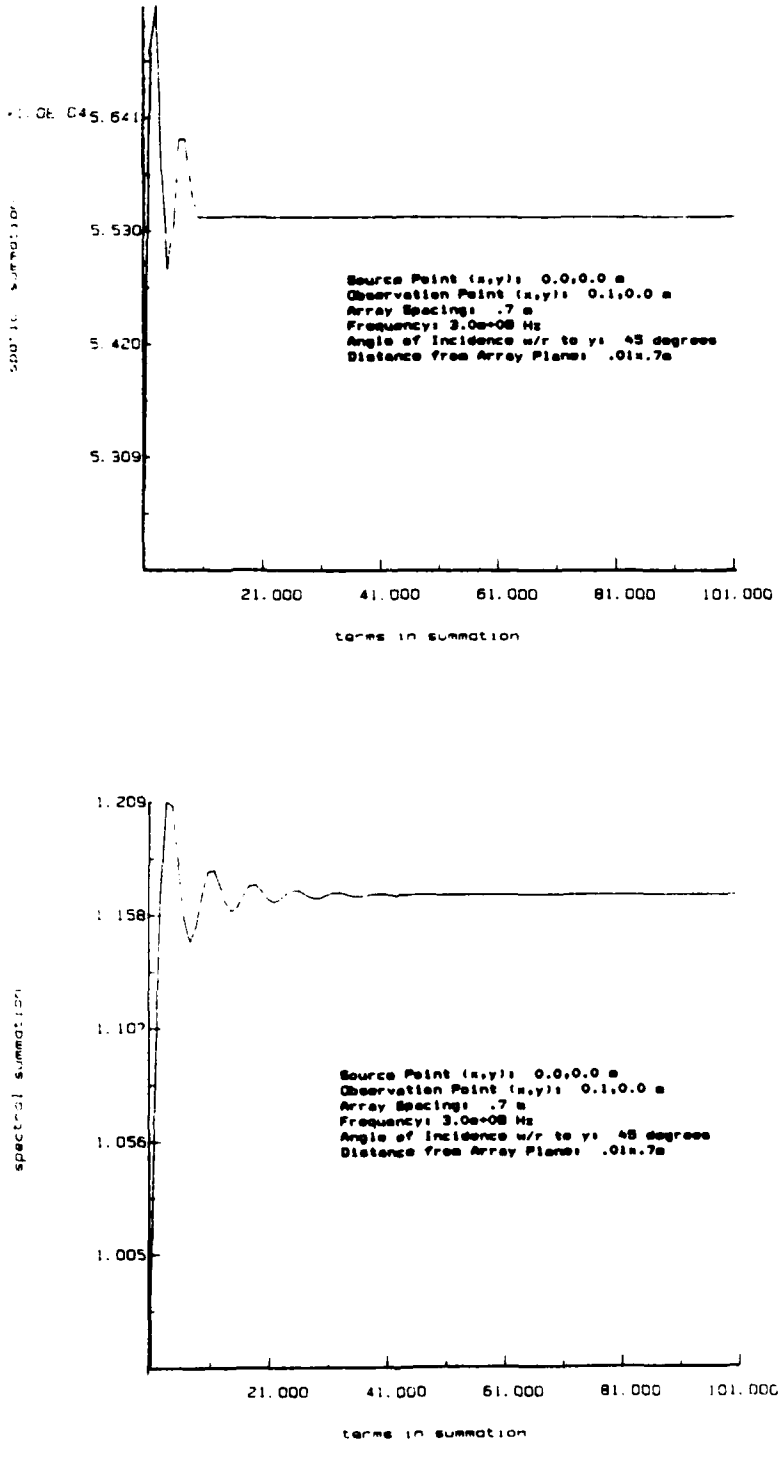

Figure 2.16 Spectral and spatial sum vs. sum limit for c=0.01

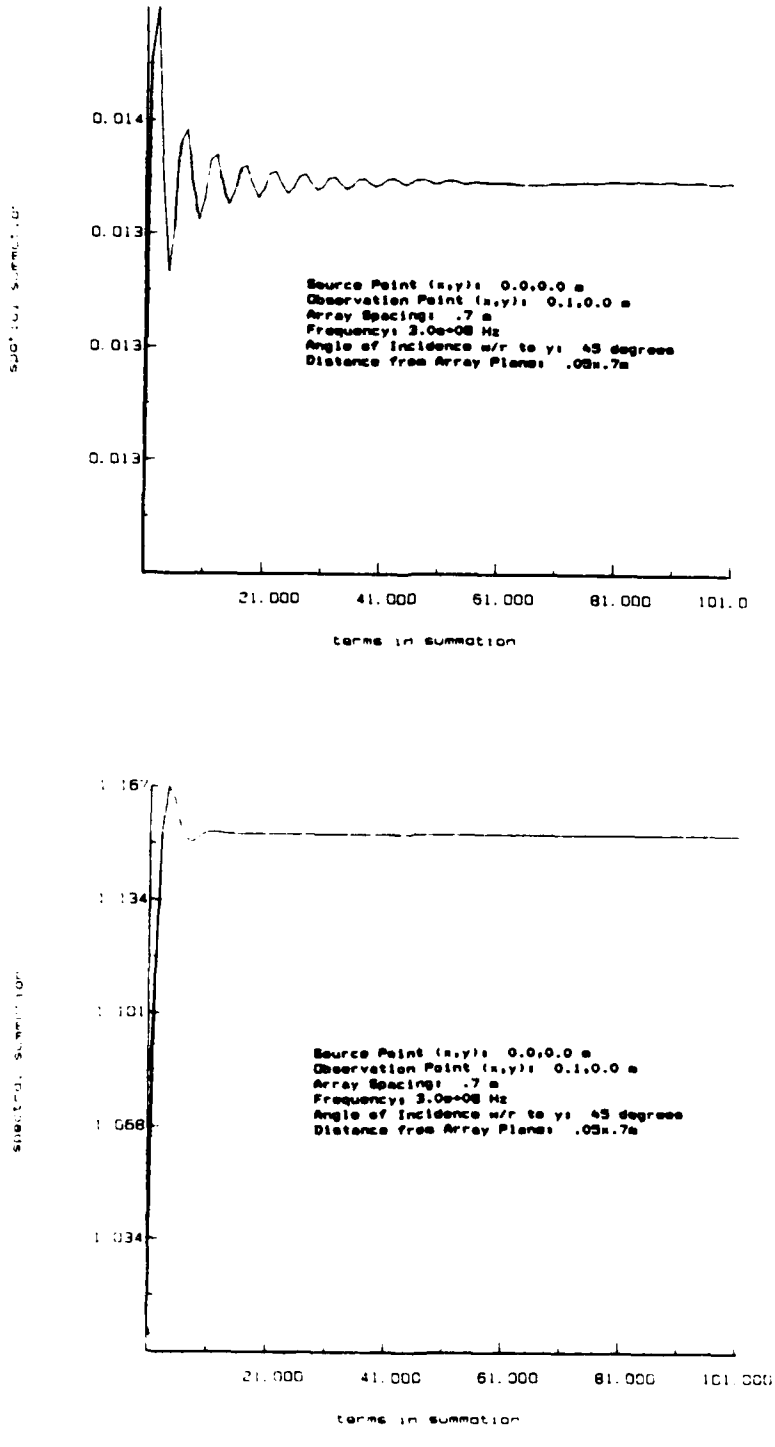

Figure 2.17 Spectral and spatial sum vs. sum limit for c=0.05

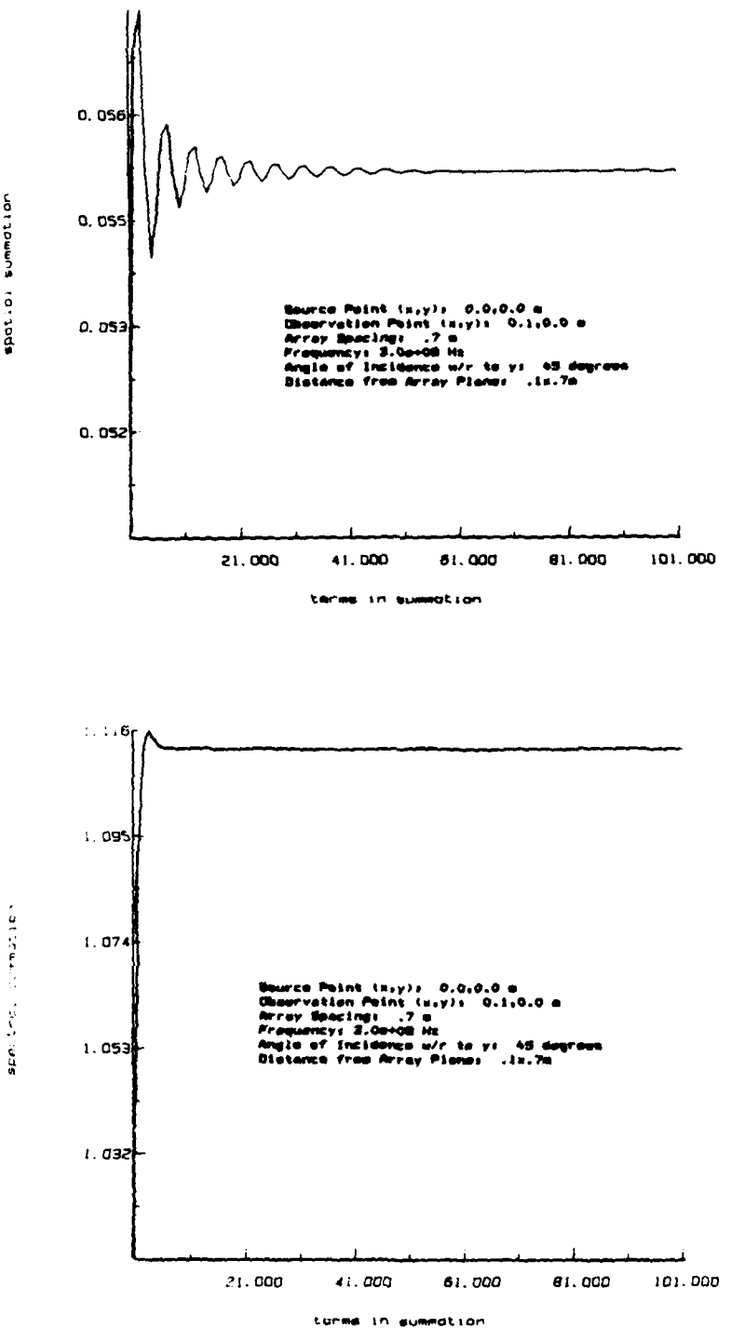

Figure 2.18 Spectral and spatial sum vs. sum limit for c=0.1

gence to a given accuracy in both domains was plotted versus c for various combinations of cell size, frequency, incident angle and test position. What emerged from this study is that although the number of terms needed for convergence changes with the parameters, the general nature of these curves remains essentially constant. Two examples are shown in Figures 2.19 and 2.20 for two different sets of parameters. When c is small, the spectral domain needs many terms to converge and the spatial domain converges immediately. As c increases, the number of spectral terms needed decreases while the number of spatial terms needed increases until at around c=0.05, the graphs cross over. The area of cross-over is relatively flat so c can be picked from the range 0.02-0.1 and both domains will be weighted approximately the same.

The true test of optimization, however, is not to minimize the total number of terms needed to perform the spectral and spatial summations as was done above, but rather to minimize the computer time needed to perform the calculation in Equation (2.46) or Equation (2.47) applied to the geometry of Figure 2.10. Prior to examining these results, Equations (2.46) and (2.47) must be discussed in greater detail.

The implementation of Equation (2.46) is subsequently called Method 1. A numerical Romberg integration routine is used to integrate the prime coordinates of G_p over the one-dimensional pulse in the unit cell. Since the test is a delta function, the convolution with the test function becomes an evaluation of $J^*[G_p]$ at the point x_T, y_T. For each s' chosen by the integration routine along the strip, the spectral and spatial summations of Equation (2.46) are summed to accuracy. First the core (m=-2:2) is summed in each domain to determine which domain is the dominant contributor to the Green's function. The dominant contributor establishes an absolute accuracy of the summations to minimize the time spent in computing a summation that has an insignificant contribution to the integrand. When the test is coincident with the basis function, the singularity is removed from the $H_0^2(k_\rho|x-x'-mb|)$ term and computed analytically. The singularity does not occur in

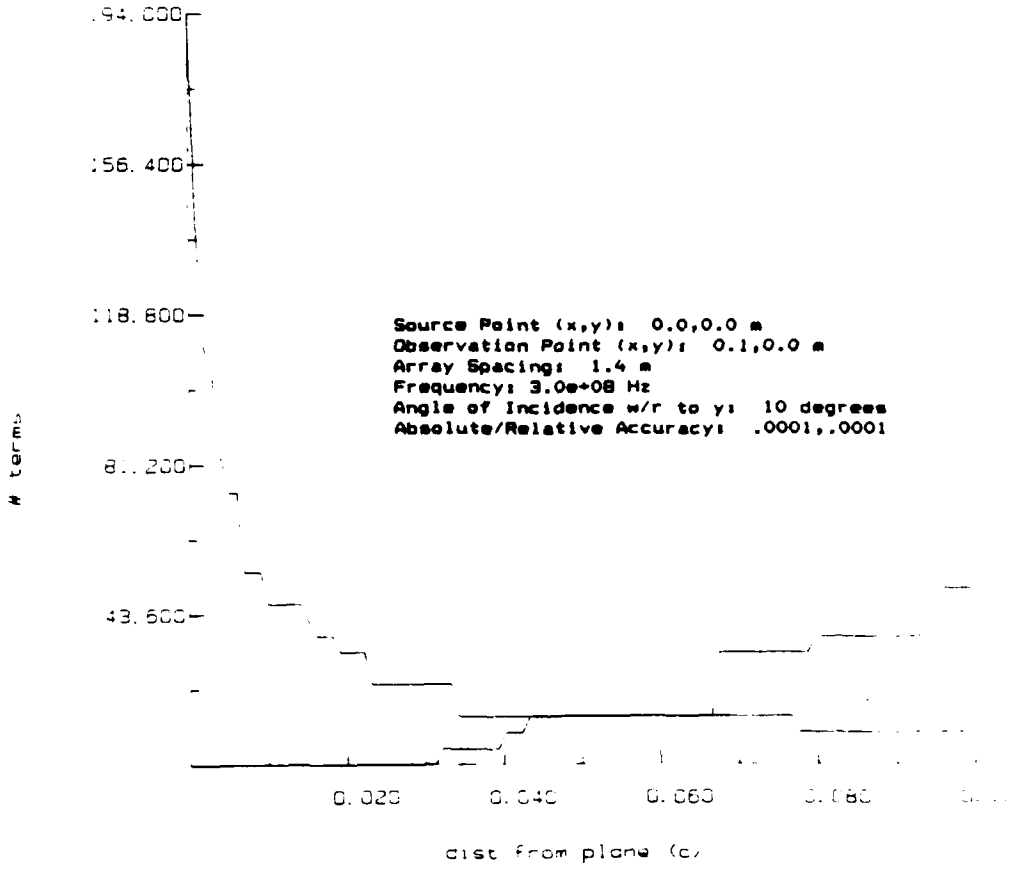

Figure 2.19 Number of terms needed for spatial and spectral sum to converge vs. c

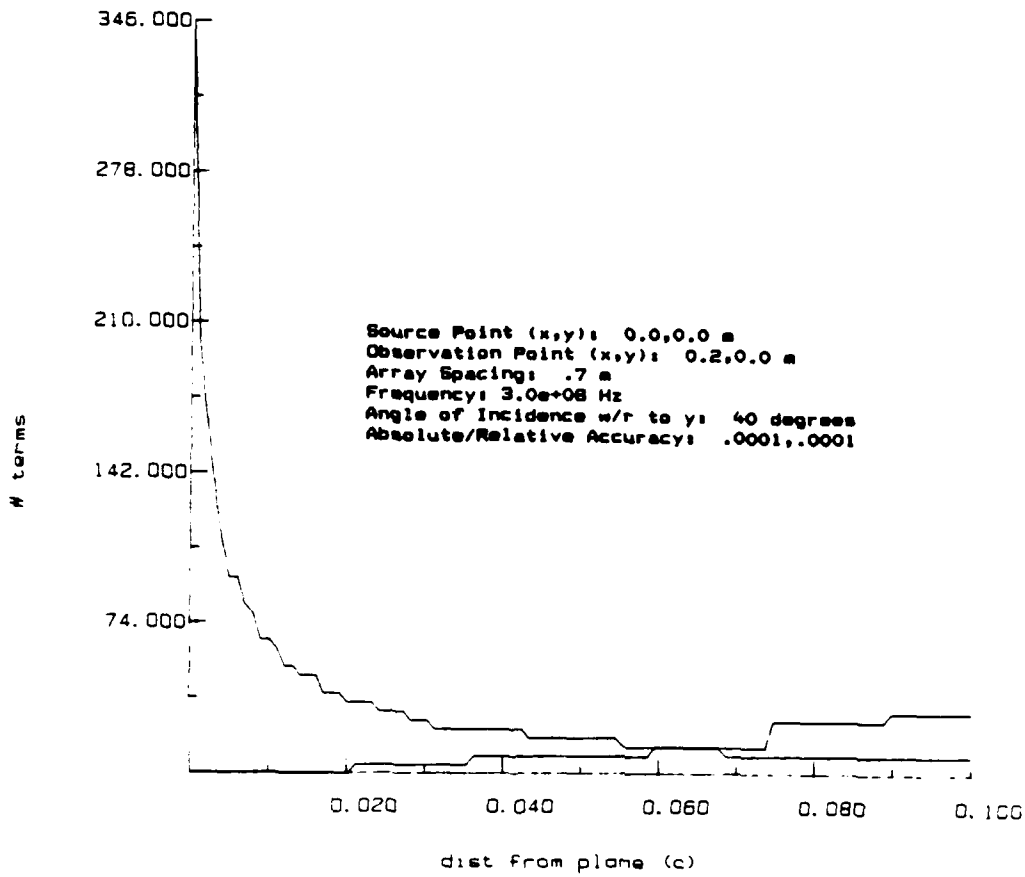

Figure 2.20 Number of terms needed for spatial and spectral sum to converge vs. c

the asymptotic terms since $c>0$.

The implementation of Equation (2.47) is subsequently termed Method 2. In this method, the basis and testing functions are distributed onto the spatial and spectral domain, i.e.,

$$\int T(s)\cdot\int J(s')\frac{1}{4j}\sum_{m=-\infty}^{\infty}e^{-jk_x mb} \tag{2.49}$$

$$\left[H_0^2\left[k_0\sqrt{(x_0-x'-mb)^2+(y_0-y')^2}\right]-H_0^2\left[k_0\sqrt{(x_0-x'-mb)^2+(|y_0-y'|+cb)^2}\right]\right]ds'ds$$

$$+\frac{1}{b}\sum_{m=-\infty}^{\infty}\int\tilde{T}(\beta_x,y)\int\tilde{J}(\beta_x,y')\frac{e^{-j(|y_0-y'|+cb)\beta_y}}{2j\beta_y}dy'dy$$

The spatial domain integrals are done numerically, as in Method 1, while the spectral domain integrals are performed analytically. When no overlap exists between $\tilde{J}$ and $\tilde{T}'$ in y (see Figure 2.21), the spectral domain sum becomes

$$\frac{1}{b}\sum_{m=-\infty}^{\infty}\frac{1}{j\beta_y}\frac{\sin(\beta_{xm}\cos\theta\pm\beta_y\sin\theta)\frac{\Delta}{2}}{(\beta_{xm}\cos\theta\pm\beta_y\sin\theta)}e^{+j(\beta_{xm}x_T-\beta_y|y_T|)}\quad y_T\lessgtr 0 \tag{2.50}$$

When $\tilde{J}$ and $\tilde{T}'$ do overlap in y, the spectral domain summation becomes

$$\frac{1}{b}\sum_{m=-\infty}^{\infty}\left\{e^{-j\beta_y y_T}\left|\frac{e^{+jA_1\frac{\Delta}{2}}-e^{-jA_1\frac{y_T}{\sin\theta}}}{jA_1}\right|+e^{+j\beta_y y_T}\left|\frac{e^{-jA_2\frac{y_T}{\sin\theta}}-e^{-jA_2\frac{\Delta}{2}}}{jA_2}\right|\right\}\frac{e^{+j\beta_{xm}x_T}}{2j\beta_y} \tag{2.51}$$

$$A_1=\beta_{xm}\cos\theta-\beta_y\sin\theta$$

$$A_2=\beta_{xm}\cos\theta+\beta_y\sin\theta$$

Note that when overlap exists between the basis and test functions, certain terms of Equation (2.51) decay as $1/\beta_y^2$ and have no exponential decay. In order to obtain exponential convergence, therefore, it is necessary to move "off plane" enough so that no overlap occurs between the basis and test functions. In Method 1, the asymptotic test point ($|y_0-y'|+cb$) was redefined for every point called by the integration routine because the spectral and spatial contributions were integrated together. In Method 2, the asymptotic test point must be fixed for the entire calculation because the spectral and spatial contribu-

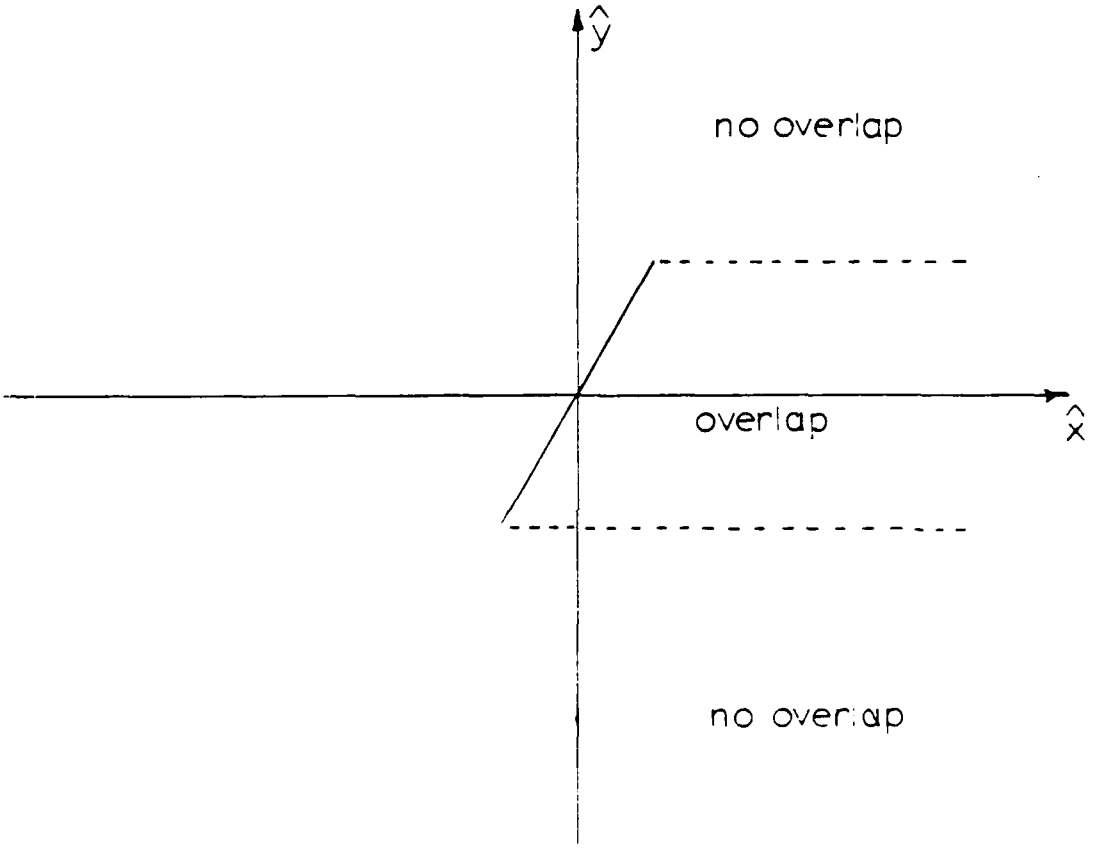

Figure 2.21 Overlap and no overlap regions for rotated strips

tions are integrated separately. This means that in Method 2, it is possible for the asymptotic terms to be singular if c is chosen such that $\sqrt{(x_0-x'-mb)^2+(|y_0-y'|+cb)^2}$ falls on the basis function as shown in Figure 2.21.

Method 3 is similar to Method 2 except that the current pulse in the spatial domain integral outside a core region (m=-1:1) is approximated as a delta function weighted by the support of the pulse. Inside the core, where the integrand varies quickly, the integration is performed numerically. Equation (2.49) becomes

$$\int T(s_k)\int J(s_l')\frac{1}{4j}\sum_{m=-1}^{+1} e^{-jk_x mb} \tag{2.52}$$

$$\left|H_0^2\left(k_0\sqrt{(x-x'-mb)^2+(y-y')^2}\right)-H_0^2\left(k_0\sqrt{(x-x'-mb)^2+(|y-y'|+cb)^2}\right)\right|$$

$$+\frac{\Delta}{4j}\sum_{m\neq-1,0,+1} e^{-jk_x mb}$$

$$\left|H_0^2\left(k_0\sqrt{(x_k-x_l-mb)^2+(y_k-y_l)^2}\right)-H_0^2\left(k_0\sqrt{(x_k-x_l-mb)^2+(|y_k-y_l|+cb)^2}\right)\right| -$$

$$+\frac{1}{b}\sum_{m=-\infty}^{\infty}\int\tilde{T}^*(\beta_{xm},y)\int\tilde{J}(\beta_{xm},y')\frac{1}{2j\beta_y}e^{-j\beta_y(|y-y'|+cb)}$$

Figures 2.22-2.26 show the time needed to compute the convolution of basis, test and periodic Green's functions using Methods 1,2 and 3 when the strips are flat ($\theta = 0^o$). As in Figures 2.19 and 2.20, although the calculation time changes with parameters such as test location, frequency, array spacing and incident angle, the shape of the curves remains essentially the same. Method 3 is the fastest method regardless of the parameters, but since it involves an approximation in the spatial domain, it is not as accurate as Methods 1 and 2. This inaccuracy becomes more pronounced as c increases and the spatial domain gets more weight. Method 1 shows a shape predicted by Figures 2.19 and 2.20. If c is too small ($c<0.01$), too much time is spent summing the spectral domain and the required time for the calculation increases. As c increases ($0.01<c<0.08$), the time goes to a minimum then slowly increases as the spatial domain becomes over-weighted.

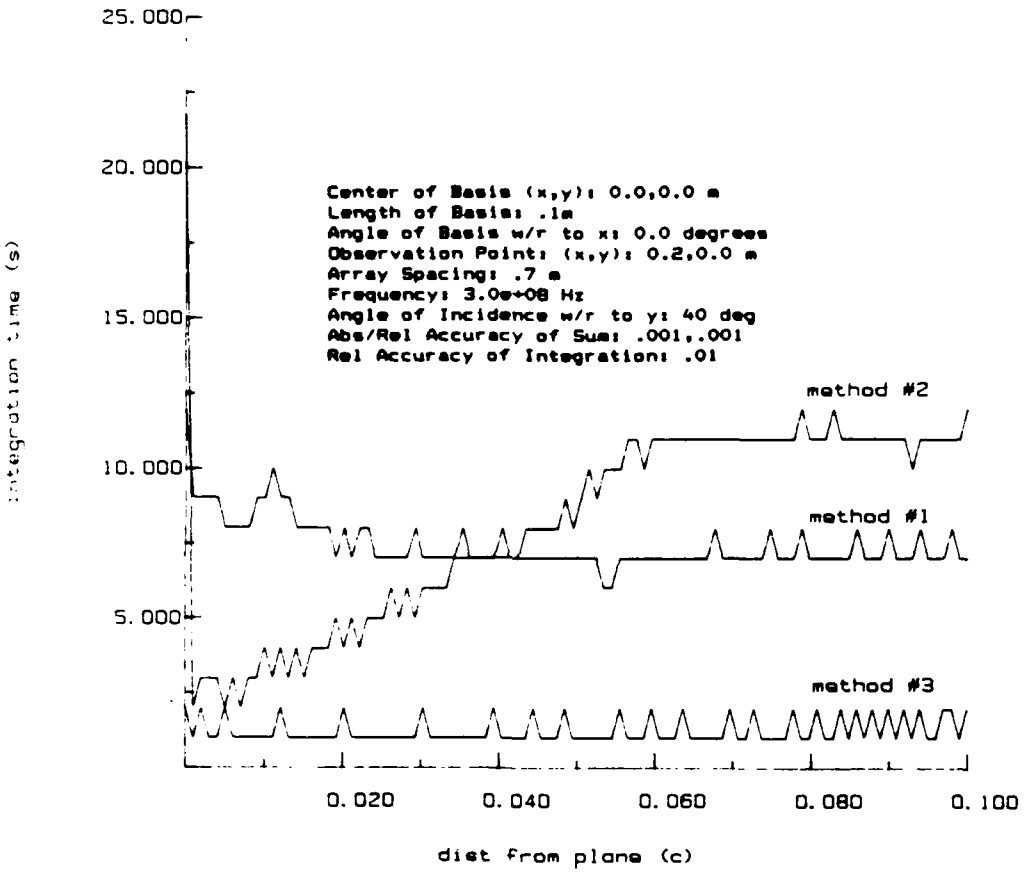

Figure 2.22 Time required for Methods 1.2 and 3 vs. c (flat case)

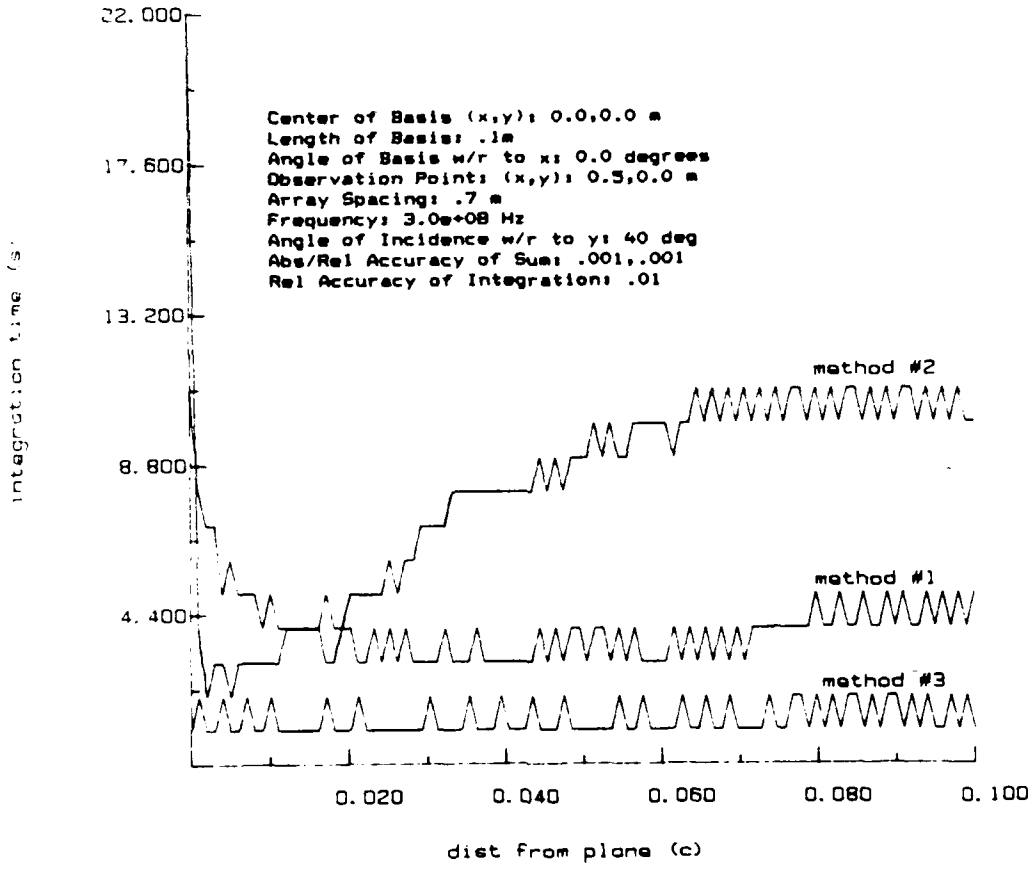

Figure 2.23 Time required for Methods 1.2 and 3 vs. c (flat case)

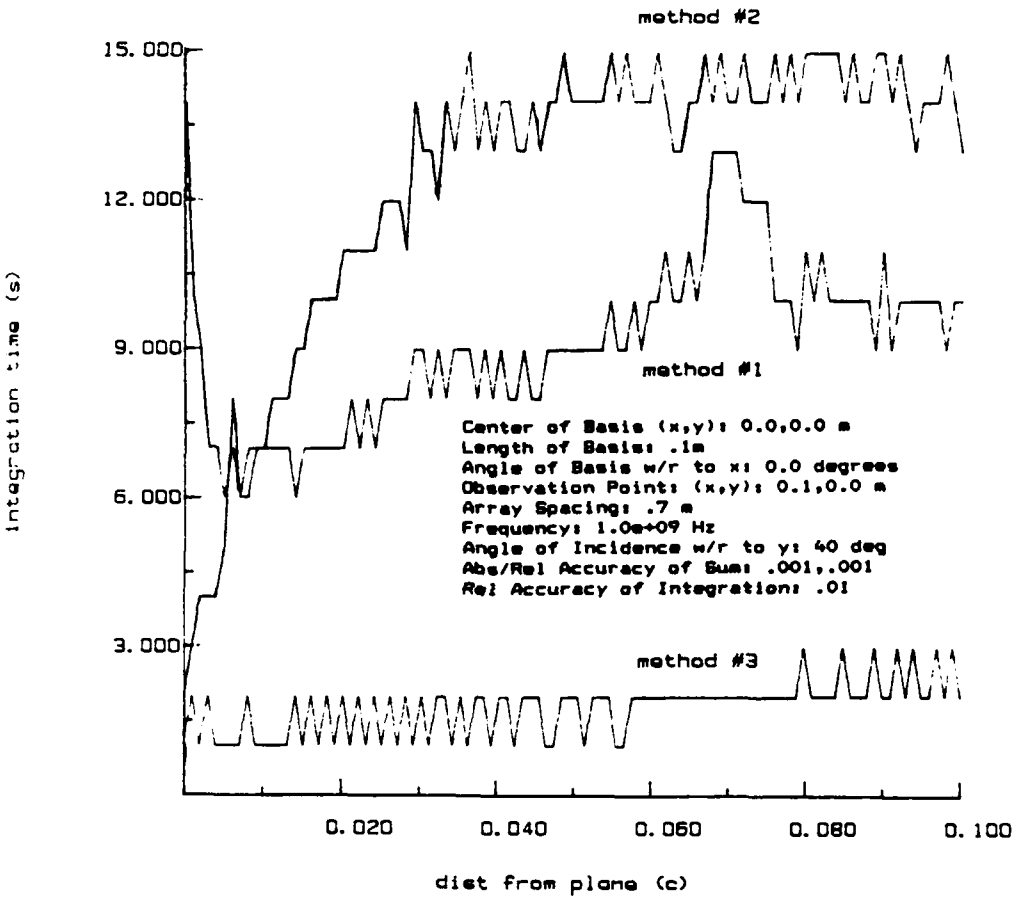

Figure 2.24 Time required for Methods 1,2 and 3 vs. c (flat case)

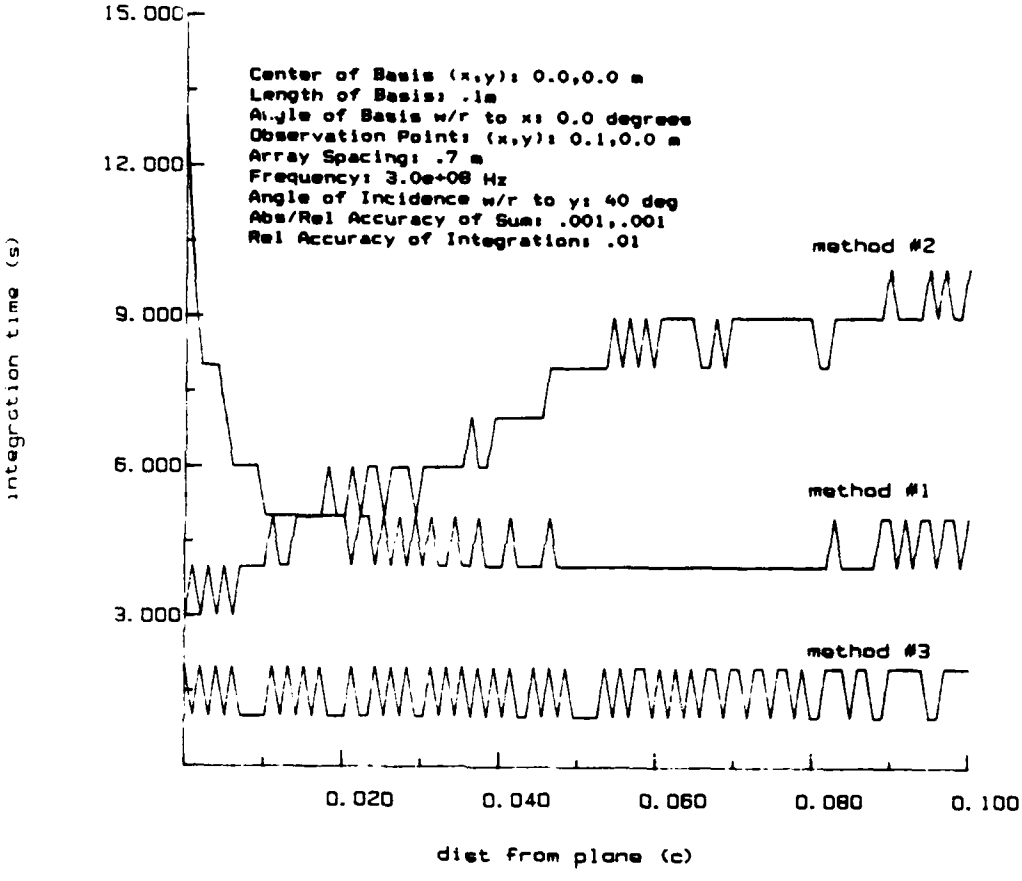

Figure 2.25 Time required for Methods 1.2 and 3 vs. c (flat case)

The time requirements for Method 2 are similar to the requirements for Method 3 for small c but increase with increasing c, crossing over Method 1 at around c=0.02. Method 2 time is dominated by the time needed to integrate numerically in the spatial domain. Although Method 2 has a simpler integrand than Method 1, it is difficult to specify an absolute accuracy correctly for the summation in Method 2. The accuracy is overspecified in Method 2 and, therefore, requires more time than Method 1. In Figure 2.26, at c=0.077, Method 2 exhibits a time spike. This occurs because the real part of the spatial integral is approximately zero, and the Romberg integration routine calls the integrand many times in order to get a sufficient degree of relative accuracy. As seen in Figures 2.27 and 2.28, the integrand itself is very smooth and the large number of calls is unnecessary. An absolute accuracy parameter could be specified in the integration routine to alleviate this problem, but this was not done.

The self-term, shown in Figure 2.29, deserves special consideration. Methods 2 and 3 exhibit the same behavior as before. Method 1 takes far more time for $c<0.01$ than could be explained by saying that the spectral sum is overweighted. The explanation for this behavior comes from an examination of the integrand. When c is close to the strip, the integrand is ill-behaved, as shown in Figure 2.30. The singularity has been subtracted only from the nonasymptotic term in the Green's function. When c is small, however, the asymptotic terms are also tending to be singular. Moving "off plane" a bit more, as shown in Figure 2.31, causes the integrand to become better behaved.

When the strip is rotated ($\theta = 45^{\circ}$), the sum has essentially the same behavior as in the flat case with the exception of two features (see Figure 2.32). The first feature is that Method 1 no longer increases in time when $c<0.01$ because since the strip is rotated, most of the points called by the integration routine are farther "off plane" than the specified "off plane" factor. The second feature is the drop in time exhibited by both Methods 2 and 3 at c=0.05. This occurs because c has moved from "on plane," where the spectral convergence

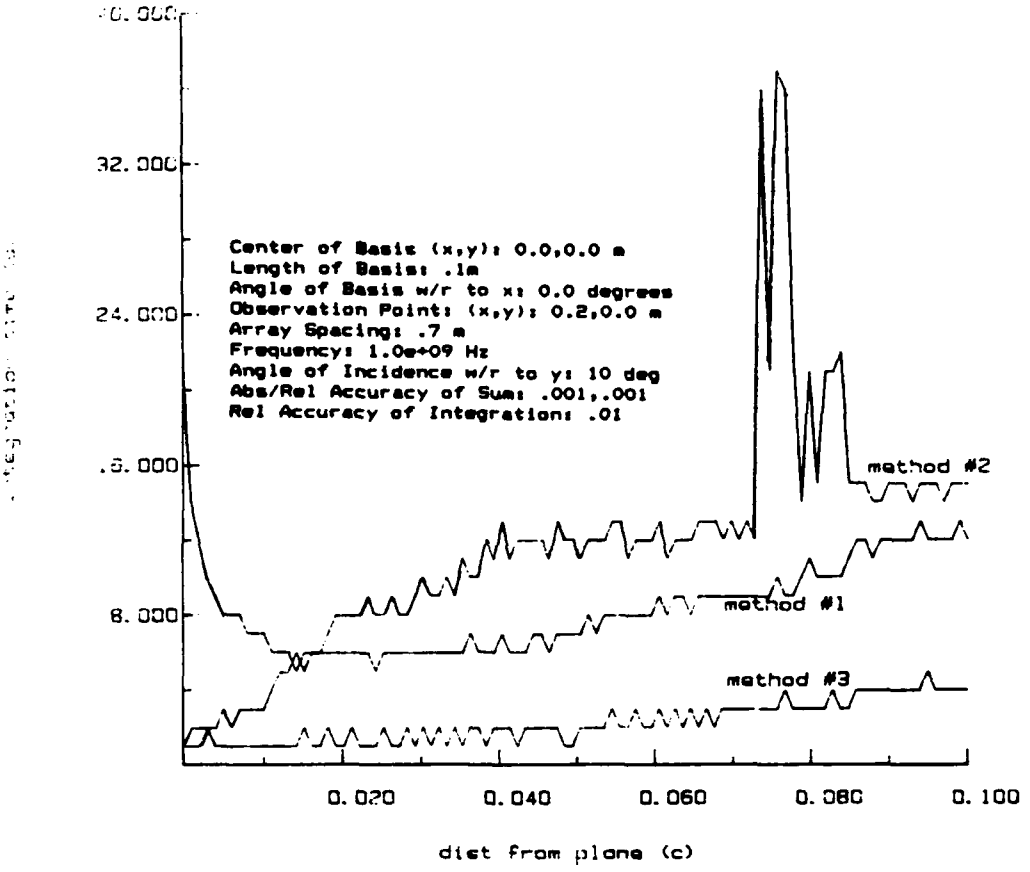

Figure 2.26 Time required for Methods 1.2 and 3 vs. c (flat case)

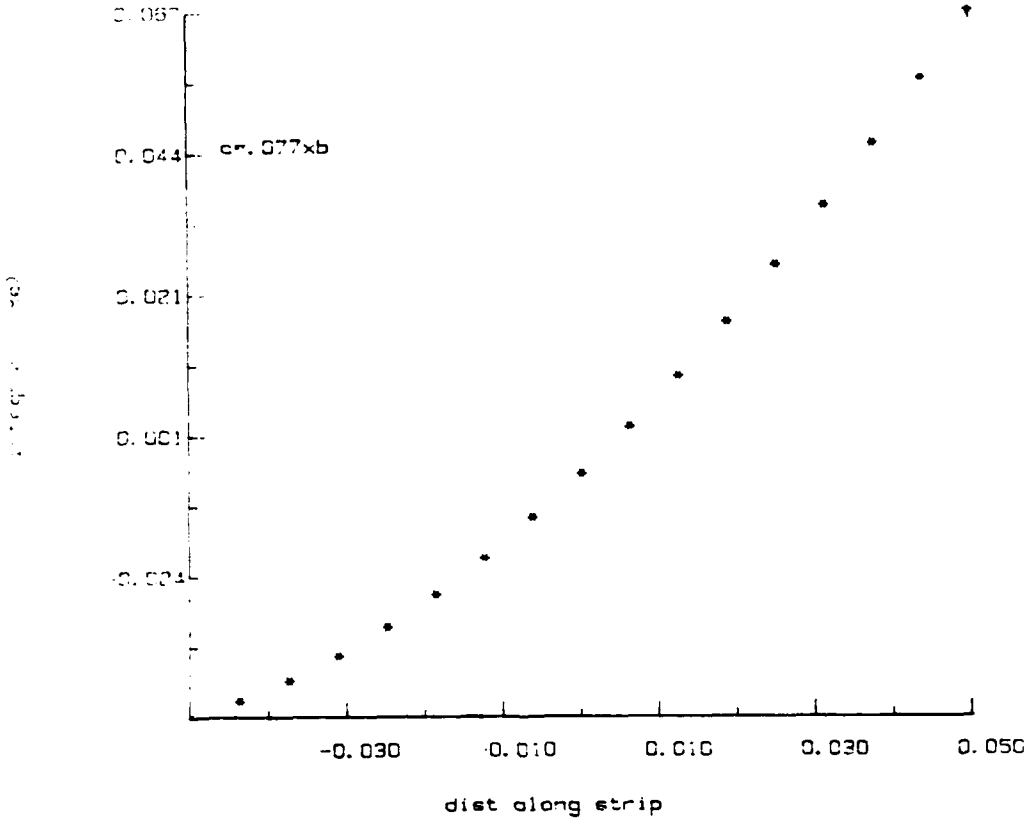

Figure 2.27 Real part of integrand for time spike in Method 2, Figure 2.26

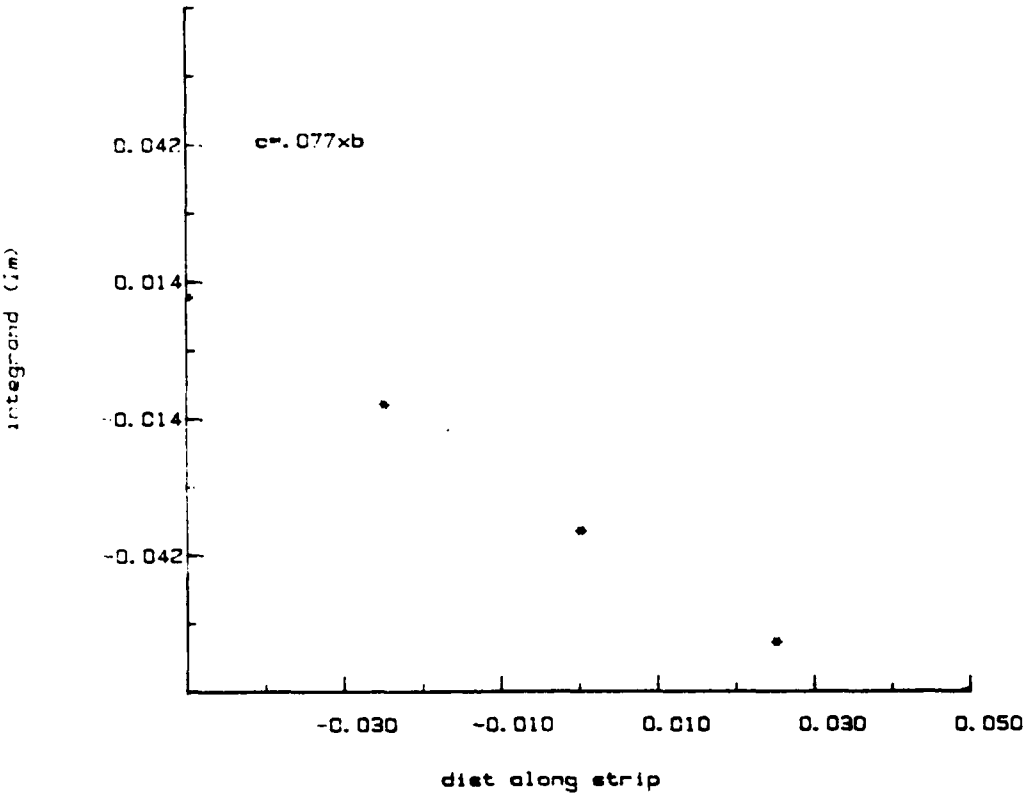

Figure 2.28 Imaginary part of integrand for time spike in Method 2. Figure 2.26

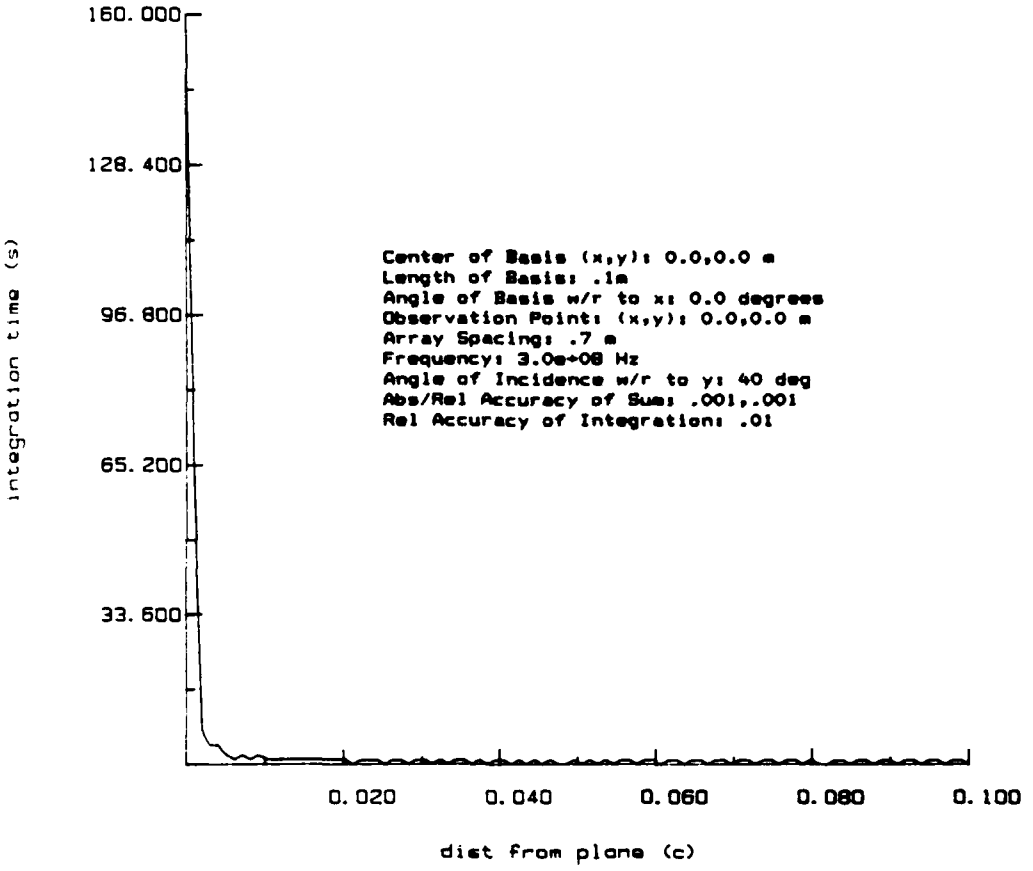

Figure 2.29 Method 1 time for the self term vs. c

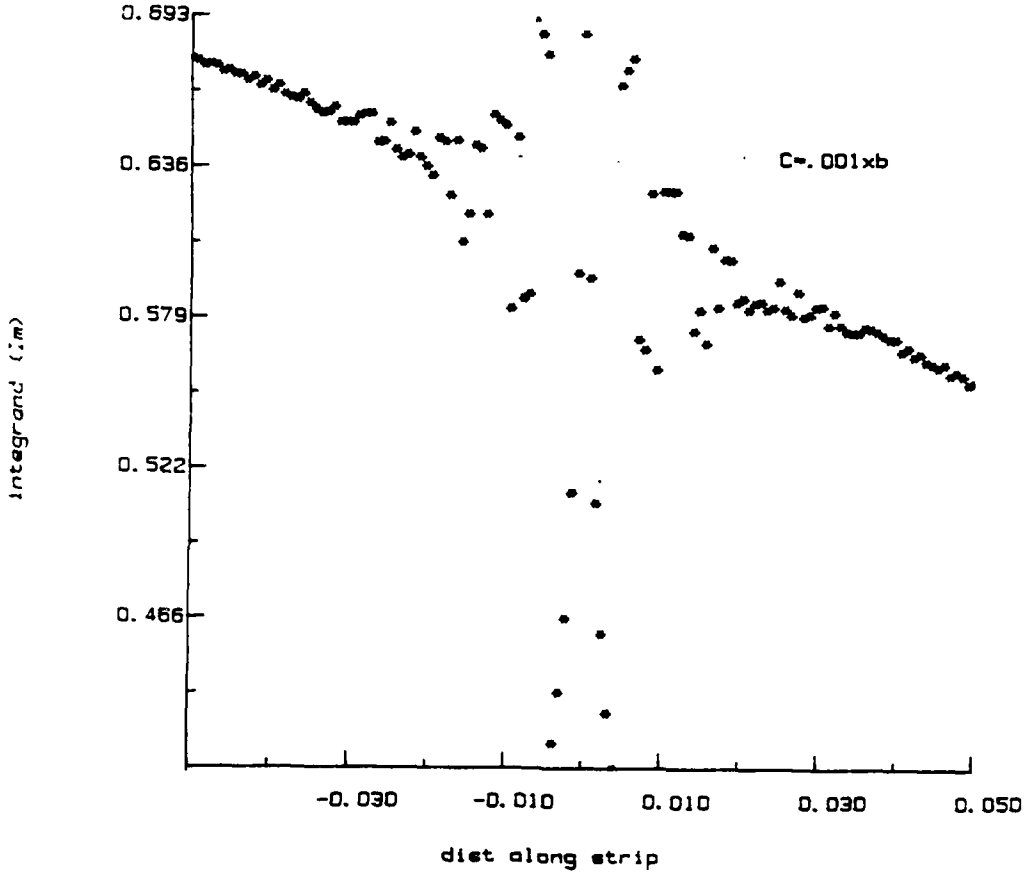

Figure 2.30 Poorly behaved integrand for c=0.001 in Figure 2.29

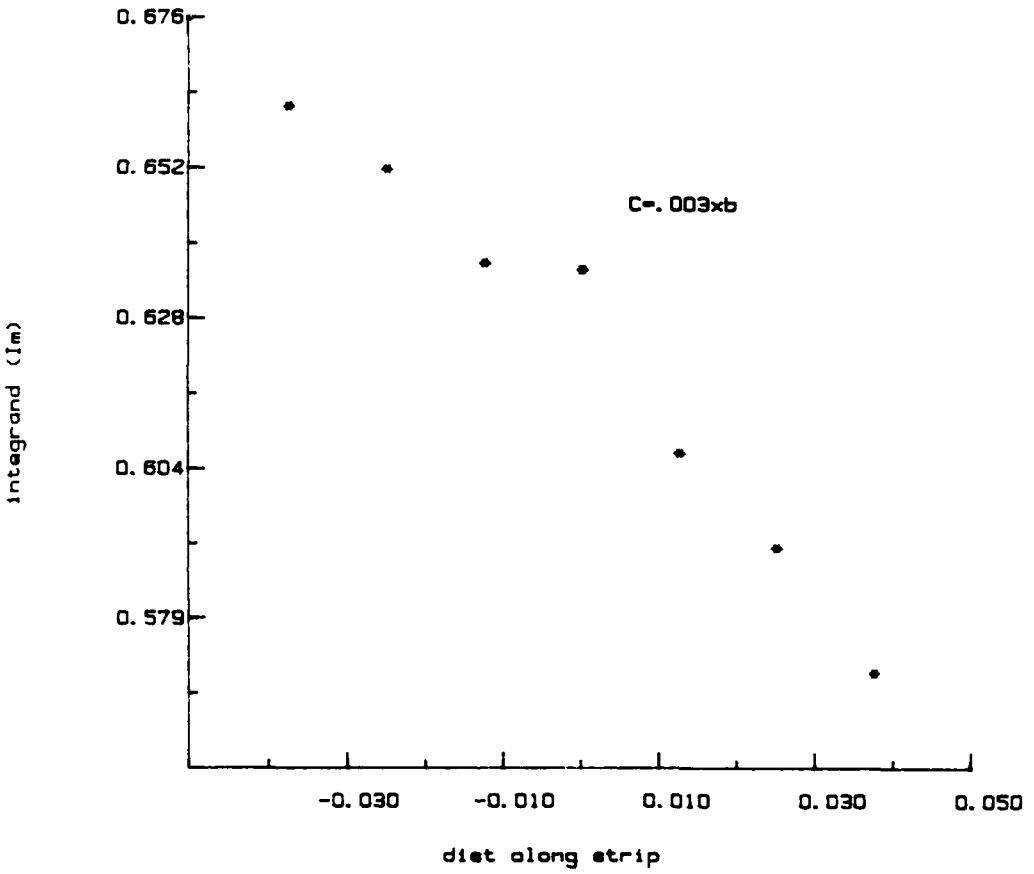

Figure 2.31 Better behaved integrand for c=0.003 in Figure 2.29

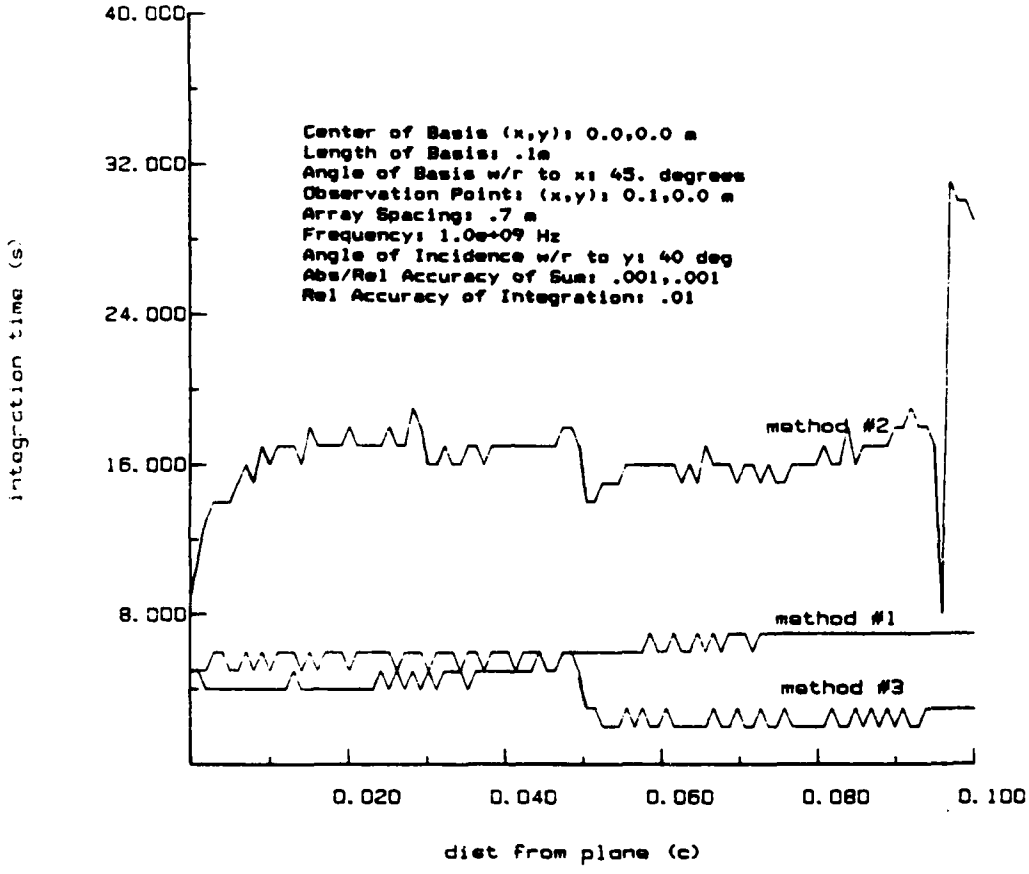

Figure 2.32 Time required for Methods 1,2 and 3 vs. c (rotated case)

behaves as $1/\beta_y^2$ to "off plane" ($c \times .7 > .05 sin(45^o)$) where the convergence is exponential.

As c approaches zero in Method 2, the accuracy of the sum must be specified more precisely because the sum is behaving as $1/m^2$ with no exponential decay. To study the region when c approaches zero, Method 2 was summed until four digits of accuracy were obtained in the final answer for all c. The result is shown for a flat strip ($\theta = 0^o$) case in Figure 2.33 and for a rotated ($\theta = 45^o$) case in Figure 2.34. For the flat case, the best choice for c was found to be c=0 for the given size of basis and testing functions. No weighting in the spatial domain is necessary for Method 2, because the smoothness of the basis and testing functions help convergence for all combinations of these functions. Since the convolution is done analytically in the spectral domain, there is no numerical integration involved. When $c \neq 0$, a numerical integration must be performed which dominates the calculation in time even though the contribution from the integration is small. In the rotated case, the best choice for c is $0.05 < c < 0.15$. Here, smoothness of basis and testing functions does not help convergence in the spectral domain. In order to get exponential convergence, we must go "off plane" ($c > 0.05$). In this case the time needed for numerical integration does not outweigh the time needed to sum in the spectral domain accurately.

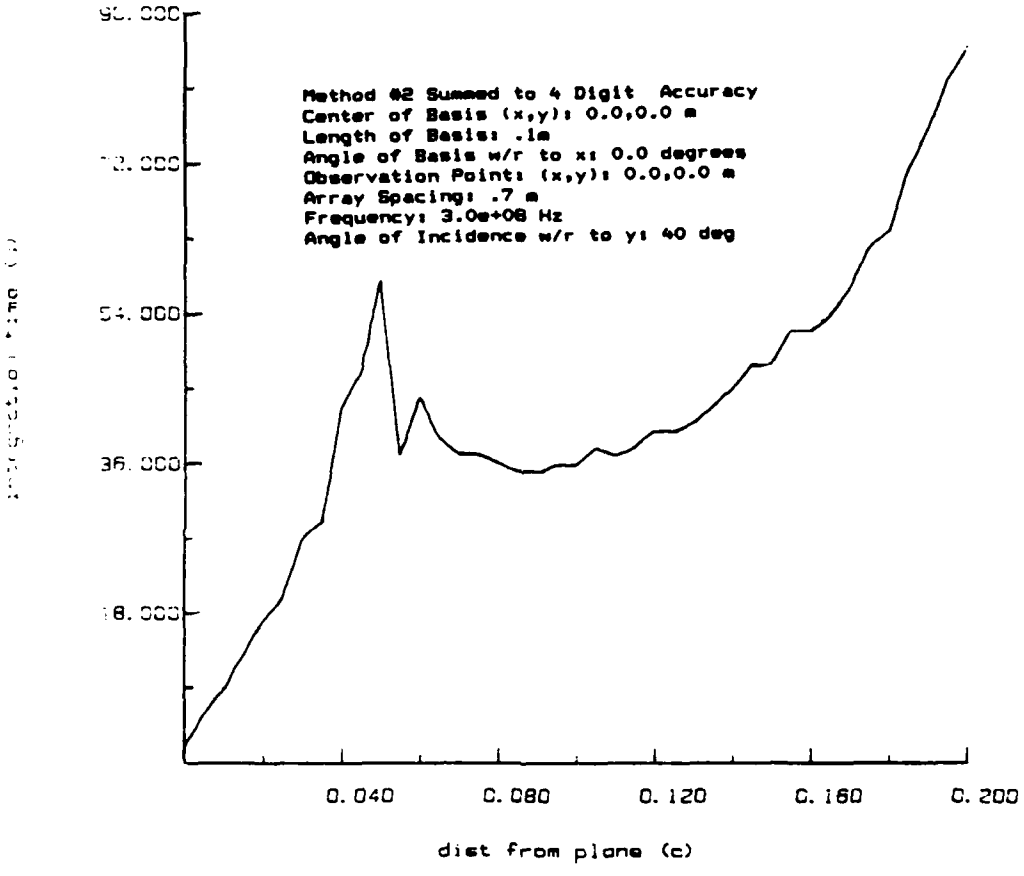

Figure 2.33 Time required for Method 2 vs. c for 4 digit accuracy (flat case)

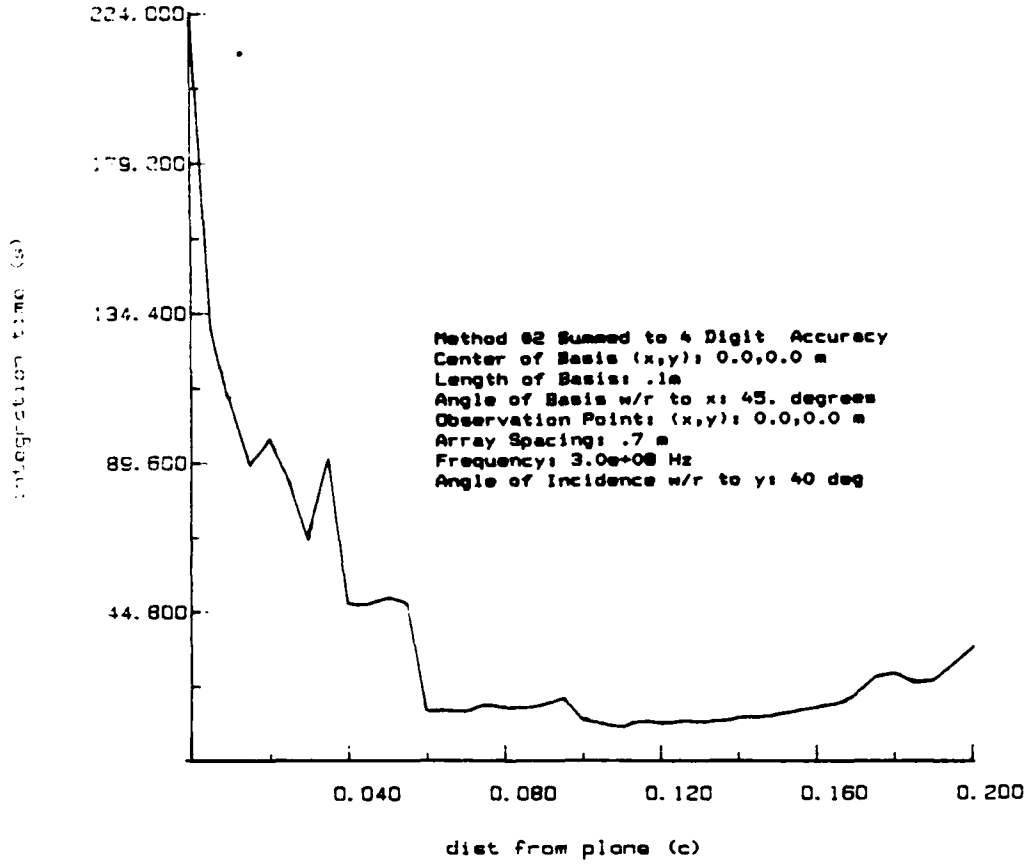

Figure 2.34 Time required for Method 2 vs. c for 4 digit accuracy (rotated case)

3. THE TWO-DIMENSIONAL ARRAY

3.1 Introduction

In this chapter, the concepts developed in Chapter 2 will be extended to examine the formulation of scattering from the two-dimensional array of plates shown in Figure 3.1. The plates are aligned perpendicularly to the xy plane and rotated to make an angle θ with respect to the $\hat{x}$ axis. The plates are arranged along a skewed axis $\hat{S}_1$ and $\hat{S}_2$. The incident field is a plane wave with a direction of propagation θ_i with respect to $\hat{z}$ and ϕ_i with respect to $\hat{x}$

3.2 Definition of Terms

The Fourier transform needed for the two-dimension array is

$$\tilde{F}(\beta_x, \beta_y) = \int\int f(x,y) e^{-j(\beta_x x + \beta_y y)} dx dy \tag{3.1a}$$

$$f(x,y) = \frac{1}{(2\pi)^2} \int\int \tilde{F}(\beta_x, \beta_y) e^{+j(\beta_x x + \beta_y y)} d\beta_x d\beta_y \tag{3.1b}$$

where f(x,y) is the function in the space domain and $\tilde{F}(\beta_x, \beta_y)$ is the Fourier transform of f(x,y) into the spectral domain.

The spatial lattice for this problem is shown in Figure 3.2 is defined by use of a translation vector $\vec{\rho}_{mn}$

$$\vec{\rho}' = \vec{\rho} + \vec{\rho}_{mn} \tag{3.2}$$
$$= \vec{\rho} + m\hat{S}_1 + n\hat{S}_2$$

where $\hat{S}_1$ and $\hat{S}_2$ are the primitive vectors defined as

$$\hat{S}_1 = c\hat{y} \tag{3.3a}$$

$$\hat{S}_2 = d\cos\Omega\hat{x} + d\sin\Omega\hat{y} \tag{3.3b}$$

Therefore, the translation vector in Cartesian coordinates is

$$\vec{\rho}_{mn} = (nd\cos\Omega)\hat{x} + (mc + nd\sin\Omega)\hat{y} \tag{3.4}$$

The reciprocal lattice is defined through the use of a reciprocal translation vector $\vec{K}_{mn}$.

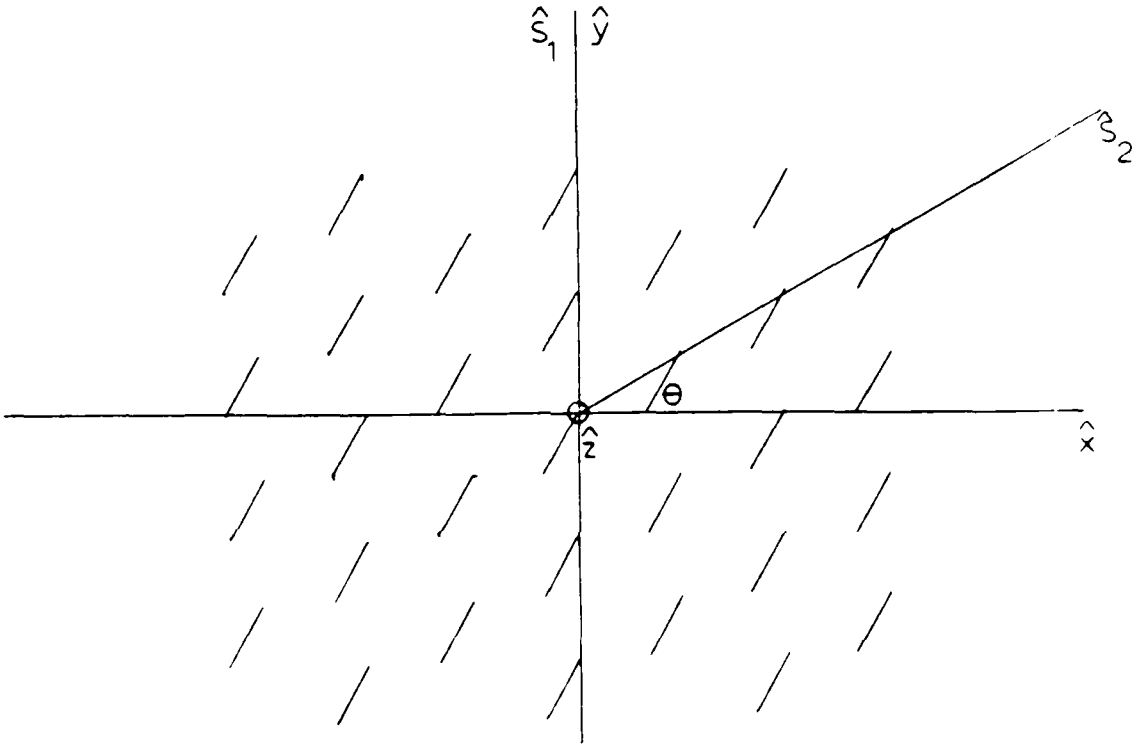

Figure 3.1 Geometry of two-dimensional array of plates

$$\vec{K}' = \vec{K} + \vec{K}_{mn} \tag{3.5}$$

$$= \vec{K} + m\tilde{S}_1 + n\tilde{S}_2$$

The reciprocal primitive lattice vectors, $\tilde{S}_1$ and $\tilde{S}_2$, are defined such that

$$\hat{S}_1 \cdot \tilde{S}_1 = 2\pi \quad \hat{S}_2 \cdot \tilde{S}_1 = 0 \tag{3.6}$$

$$\hat{S}_1 \cdot \tilde{S}_2 = 0 \quad \hat{S}_2 \cdot \tilde{S}_2 = 2\pi$$

Therefore,

$$\tilde{S}_1 = \frac{2\pi}{c \cos\Omega} \left| \hat{y} \cos\Omega - \hat{x} \sin\Omega \right| \tag{3.7a}$$

$$\tilde{S}_2 = \frac{2\pi}{d \cos\Omega} \hat{x} \tag{3.7b}$$

and the reciprocal translation vector in Cartesian coordinates becomes

$$\vec{K}_{mn} = 2\pi \left| \frac{n}{d \cos\Omega} - \frac{m \sin\Omega}{c \cos\Omega} \right| \hat{x} + \frac{2\pi m}{c} \hat{y} \tag{3.8}$$

The reciprocal primitive lattice vectors are shown in relation to the spatial primitive lattice vectors in Figure 3.3.

3.3 Formulation of G_p

The electric field integral equation (Equation (2.6)) will be used to analyze the doubly periodic array of plates. In this case the Green's function is defined as the vector potential response to an array of point sources. In the spatial domain, an array of point sources located at x', y', z' in each unit cell may be represented as

$$J_s(x', y', z') = \sum_{n=-\infty}^{\infty} \sum_{m=-\infty}^{\infty} \delta(\vec{\rho} - \vec{\rho}' - \vec{\rho}_{mn}) e^{-j\vec{K}' \cdot \vec{\rho}_{mn}} \delta(z - z') \tag{3.9}$$

The response at x_0, y_0, z_0 to each point source may be summed to obtain

$$G_p(\vec{r}_0, \vec{r}') = \sum_{n=-\infty}^{\infty} \sum_{m=-\infty}^{\infty} e^{-j\vec{K}' \cdot \vec{\rho}_{mn}} \frac{e^{-jk_0\sqrt{(x_0 - x' - x_{mn})^2 + (y_0 - y' - y_{mn})^2 + (z_0 - z')^2}}}{4\pi\sqrt{(x_0 - x' - x_{mn})^2 + (y_0 - y' - y_{mn})^2 + (z_0 - z')^2}} \tag{3.10}$$

In the spectral domain, a point source array may be expressed as a double summation of current sheets through the use of the Fourier transform pair (Equation (3.1)). Each of the current sheets has a period dictated by the reciprocal lattice and a cell to cell phase

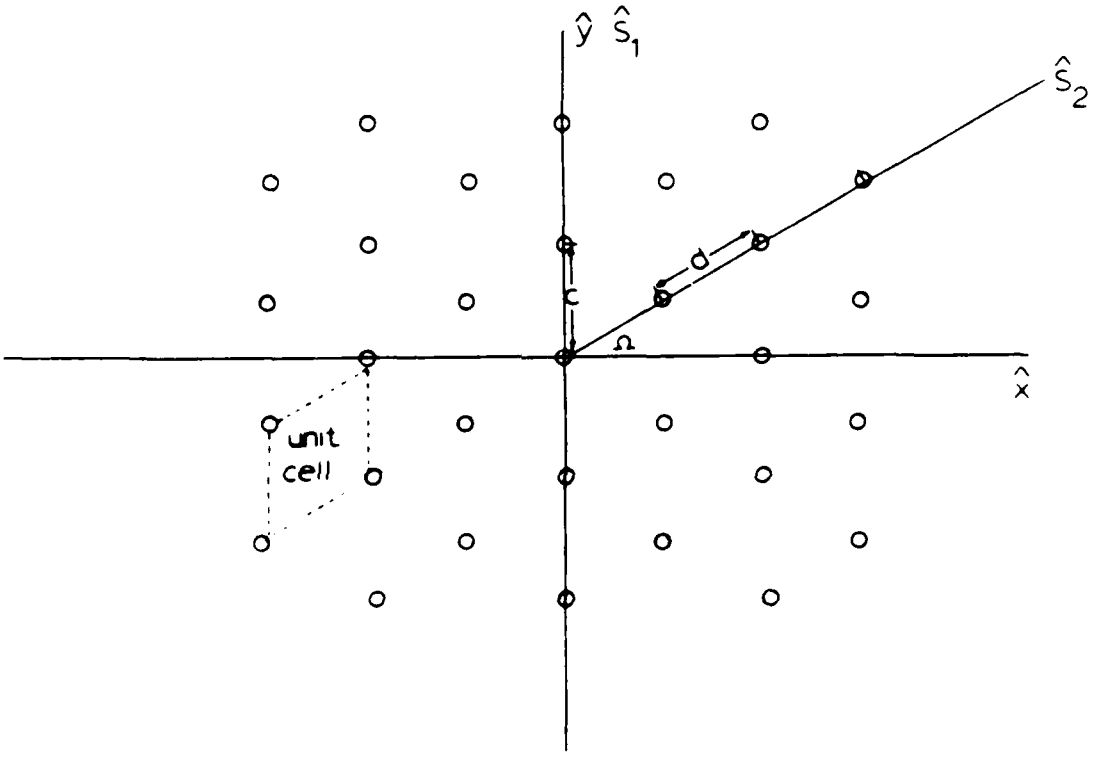

Figure 3.2 Two-dimensional spatial lattice

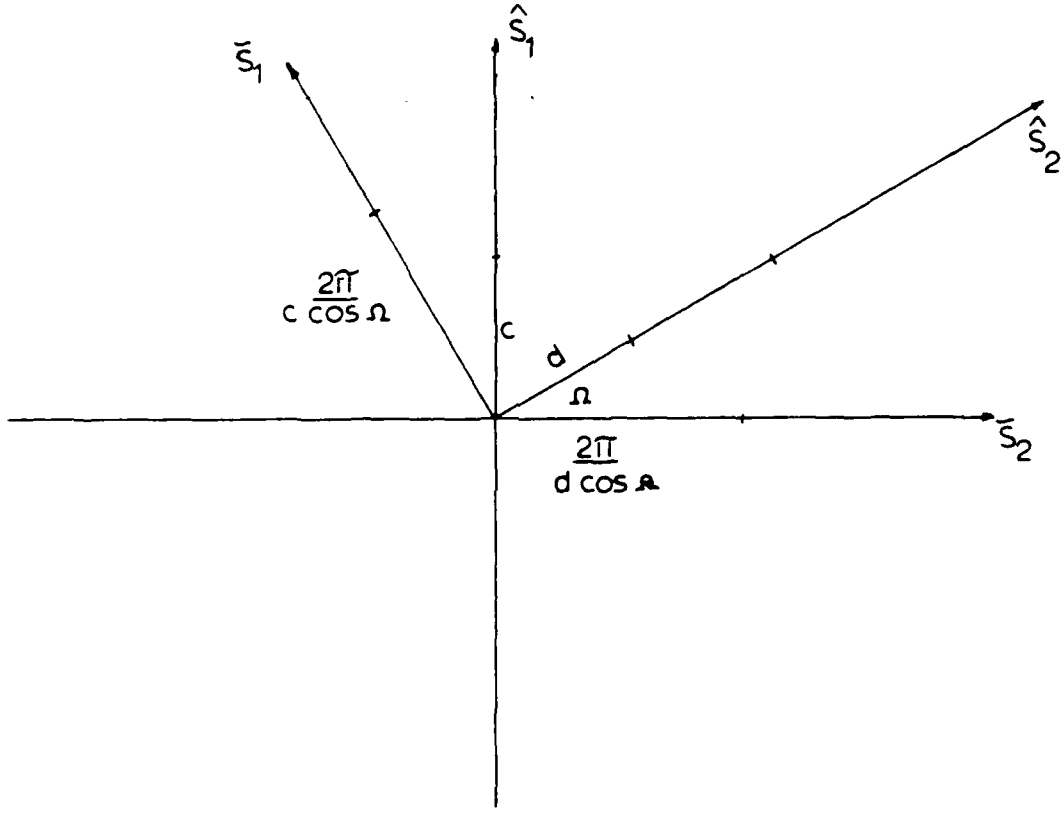

Figure 3.3 Spatial and reciprocal primitive lattice vectors

shift dictated by the incident field.

$$J_a(x,y,z) = \frac{1}{C.A.} \sum_{m=-\infty}^{\infty} \sum_{n=-\infty}^{\infty} e^{+j(\vec{K}_{mn}-\vec{k}_{inc})\cdot(\vec{\rho}-\vec{\rho}')} \delta(z-z') \tag{3.11}$$

C.A. is the area of the unit cell, $\vec{K}_{mn}$ is defined in Equation (3.8) above and $\vec{k}_{inc}$ is the propagation constant of the incident wave. Adding the response at x_0, y_0, z_0 of each current sheet the following equation is obtained:

$$G_p(\vec{r}_0|\vec{r}') = \frac{1}{C.A.} \sum_{m=-\infty}^{\infty} \sum_{n=-\infty}^{\infty} \frac{e^{-j\gamma|z_0-z'|} e^{+j(\vec{K}_{mn}-\vec{k}_{inc})\cdot(\vec{\rho}_0-\vec{\rho})}}{2j\gamma} \tag{3.12}$$

where application of the radiation condition yields

$$\gamma = \begin{cases} \sqrt{k_0^2-\beta_x^2-\beta_y^2} & \text{if } k_0^2 > \beta_x^2+\beta_y^2 \\ -j\sqrt{\beta_x^2+\beta_y^2-k_0^2} & \text{if } \beta_x^2+\beta_y^2 > k_0^2 \end{cases} \tag{3.13}$$

$$\beta_x = (\vec{K}_{mn}-\vec{k}_{inc})\cdot\hat{x} = 2\pi\left|\frac{n}{d\cos\Omega} - \frac{m\sin\Omega}{c\cos\Omega}\right| - k_x$$

$$\beta_y = (\vec{K}_{mn}-\vec{k}_{inc})\cdot\hat{y} = \frac{2\pi m}{c} - k_y$$

The spatial domain formulation of G_p converges slowly as explained in Chapter 2. The spectral formulation converges rapidly when $z_0 \neq z'$ (the "off plane" case) and converges slowly when $z_0 = z'$ (the "on plane" case). As with the strip array, since the plates are not flat on the xy plane, the derivatives of the scalar potential term may not be transferred onto the Green's function, rather the derivatives must be transferred explicitly onto the basis and testing functions. In order for the subsequent integrations to make sense, rooftop basis and razor testing function order of smoothness is chosen as shown in Figure 3.4. This is the three-dimensional analogue to the triangle basis and pulse testing functions used in Chapter 2. If both basis and test functions take a derivative, the rooftop/razor reduces to combinations of two-dimensional pulses and delta testing. For the vector potential, the rooftop is approximated as a two-dimensional pulse with the same moment as the rooftop and the razor as a delta function weighted by the support of the razor. All integrals are, therefore, reduced to the same form: the response at a point x_T, y_T, z_T due to an array of

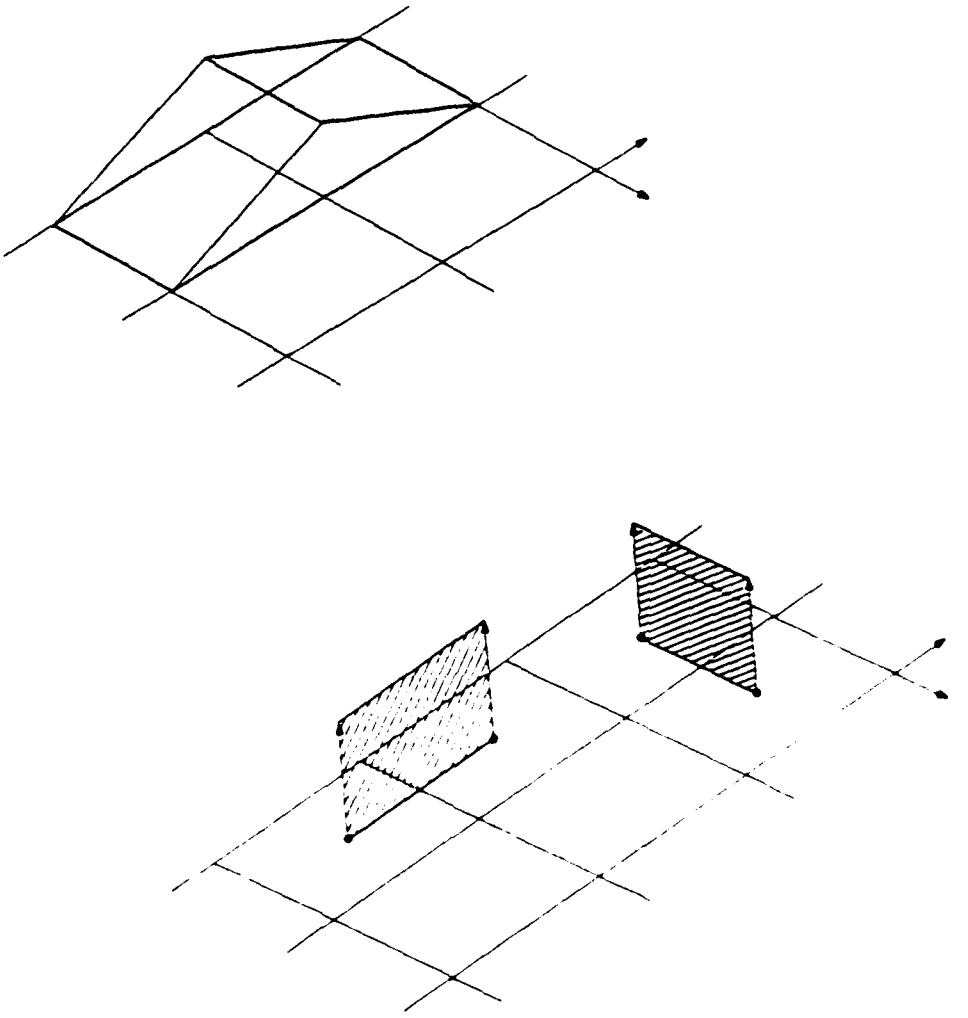

Figure 3.4 Rooftop basis and razor test functions

two-dimensional current pulses located on the spatial lattice.

3.4 Acceleration of Convergence in Spatial Domain

In order to accelerate the convergence of the spatial domain sum (Equation (3.10)), the asymptotic behavior of e^{-jkR}/R is added to and subtracted from the periodic Green's function by moving off the xy plane cCA units.

$$\sum_{m=-\infty}^{\infty}\sum_{n=-\infty}^{\infty} e^{-j\vec{k}_{inc}\cdot\vec{\rho}_{mn}} \frac{e^{-jk_0\sqrt{|\vec{\rho}_0-\vec{\rho}'-\vec{\rho}_{mn}|^2+(z_0-z')^2}}}{4\pi\sqrt{|\vec{\rho}_0-\vec{\rho}'-\vec{\rho}_{mn}|^2+(z_0-z')^2}} = \sum_{m=-\infty}^{\infty}\sum_{n=-\infty}^{\infty} e^{-j\vec{k}_{inc}\cdot\vec{\rho}_{mn}} \tag{3.14}$$

$$\left[\frac{e^{-jk_0\sqrt{|\vec{\rho}_0-\vec{\rho}-\vec{\rho}_{mn}|^2+(z_0-z')^2}}}{4\pi\sqrt{|\vec{\rho}_0-\vec{\rho}'-\vec{\rho}_{mn}|^2+(z_0-z')^2}} - \frac{e^{-jk_0\sqrt{|\vec{\rho}_0-\vec{\rho}-\vec{\rho}_{mn}|^2+(|z_0-z'|+cCA)^2}}}{4\pi\sqrt{|\vec{\rho}_0-\vec{\rho}'-\vec{\rho}_{mn}|^2+(|z_0-z'|+cCA)^2}}\right]$$

$$+\sum_{m=-\infty}^{\infty}\sum_{n=-\infty}^{\infty} e^{-j\vec{k}_{inc}\cdot\vec{\rho}_{mn}} \frac{e^{-jk_0\sqrt{|\vec{\rho}_0-\vec{\rho}-\vec{\rho}_{mn}|^2+(|z_0-z'|+cCA)^2}}}{4\pi\sqrt{|\vec{\rho}_0-\vec{\rho}'-\vec{\rho}_{mn}|^2+(|z_0-z'|+cCA)^2}}$$

The first summation remains in the spatial domain and converges rapidly because the asymptotic behavior is subtracted out. The second summation is smooth, nonsingular and slowly converging. It is brought into the spectral domain by means of Poisson summation formula.

For a two-dimensional space, Parseval's theorem is

$$\int\int h(x,y) f(x,y)\,dx\,dy = \frac{1}{4\pi^2}\int\int \tilde{H}(\beta_x,\beta_y)\tilde{F}(\beta_x,\beta_y)\,d\beta_x\,d\beta_y \tag{3.15}$$

If $h(x,y)$ is a comb function distributed along the spatial lattice with a cell to cell phase shift

$$h(x,y) = \sum_{m=-\infty}^{\infty}\sum_{n=-\infty}^{\infty} \delta(\vec{\rho}-\vec{\rho}_{mn})\, e^{-j\vec{k}_{inc}\cdot\vec{\rho}_{mn}} \tag{3.16a}$$

then $\tilde{H}(\beta_x,\beta_y)$ is also a comb function distributed along the reciprocal lattice

$$\tilde{H}(\beta_x,\beta_y) = \frac{4\pi^2}{cA}\sum_{m=-\infty}^{\infty}\sum_{n=-\infty}^{\infty} \delta(\vec{K}-\vec{K}_{mn}-\vec{k}_{inc}) \tag{3.16b}$$

Application of Parseval's theorem to the second sum of Equation (3.14) yields

$$f(x,y) = \frac{e^{-jk_0\sqrt{|\vec{\rho}_0-\vec{\rho}'|^2+(|z_0-z'|+cCA)^2}}}{4\pi\sqrt{|\vec{\rho}_0-\vec{\rho}'|^2+(|z_0-z'|+cCA)^2}} \tag{3.17a}$$

$$\tilde{F}(\beta_x,\beta_y) = \int\int \frac{e^{-jk_0\sqrt{|\vec{\rho}_0-\vec{\rho}'|^2+(|z_0-z'|+cCA)^2}}}{4\pi\sqrt{|\vec{\rho}_0-\vec{\rho}'|^2+(|z_0-z'|+cCA)^2}} e^{-j(\beta_x x+\beta_y y)}dxdy \tag{3.17b}$$

Substitution of Equations (3.16) and (3.17) into (3.15) yields

$$\frac{1}{4\pi^2}\int\int \tilde{H}(\beta_x,\beta_y)\tilde{F}(\beta_x,\beta_y)d\beta_x d\beta_y \tag{3.18}$$

$$= \frac{1}{C.A.}\sum_{m=-\infty}^{\infty}\sum_{n=-\infty}^{\infty}\frac{e^{-j\gamma|z-z'|+cCA}}{2j\gamma}e^{+j(\vec{K}_{mn}-\vec{k}_{inc})(\vec{\rho}_0-\vec{\rho})}$$

where γ is defined by Equation (3.13).

3.5 Numerical Implementation of the Spatial Domain Acceleration

As with the strip problem, the time needed to calculate the convolution of a two-dimensional current pulse with the periodic Green's function tested with a delta function was plotted for three different methods. In this section, c is multiplied by the unit cell area (C.A.).

Method 1 implements the integration of the periodic Green's function (Equation (3.14)) over a two-dimensional patch numerically using a Romberg integration routine. For every x',y',z' chosen by the routine, the spectral and spatial domains of Equation (3.14) are summed to accuracy. When the test is coincident with the basis function, the singularity is removed from the non-asymptotic term and added back in analytically. The singularity does not occur in the asymptotic terms since $c>0$. For each x',y',z', the test point of the asymptotic function moves as shown in Figure 3.5. This is allowed since the summations in the spectral and spatial domains are being done together. Figure 3.6 shows the time behavior of Method 1 for a 1mx1m basis arranged on a regular hexagonal lattice. The time required to calculate the matrix element for a plate array is similar to the time required for a strip array. If c is too small ($c<0.02$), the spectral domain is overweighted, and if c is too large ($c>0.12$), the spatial domain is overweighted. The time needed to calcu-

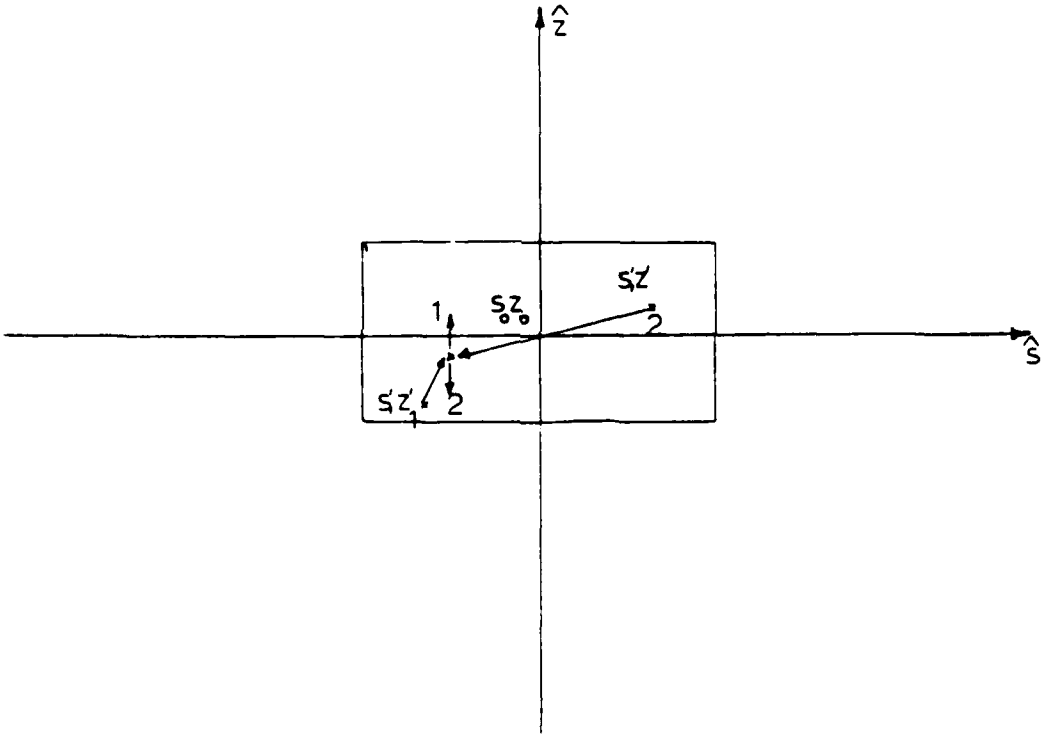

Figure 3.5 Movement of asymptotic test point in Method 1

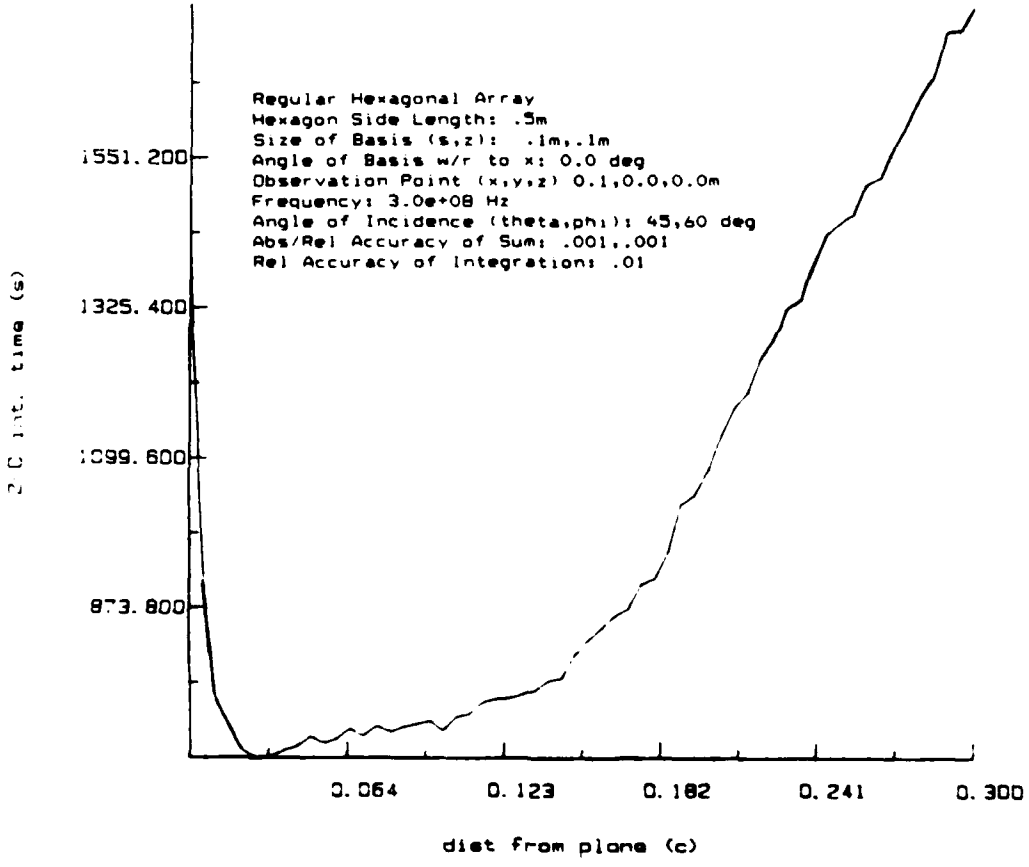

Figure 3.6 Time required for Method 1 vs. c

late the matrix element for the plate array is approximately the time needed to calculate the strip array matrix element raised to the fourth power.

Method 2 involves distributing the basis and testing functions onto the spatial and spectral domains.

$$\int T(\rho,z)\int J(\rho',z')\sum_{m=-\infty}^{\infty}\sum_{n=-\infty}^{\infty} e^{-j\vec{k}_{inc}\cdot\vec{\rho}_{mn}} \tag{3.19}$$

$$\left|\frac{e^{-jk_0\sqrt{|\vec{\rho}_0-\vec{\rho}-\vec{\rho}_{mn}|^2+(z_0-z')^2}}}{4\pi\sqrt{|\vec{\rho}_0-\vec{\rho}'-\vec{\rho}_{mn}|^2+(z_0-z')^2}}-\frac{e^{-jk_0\sqrt{|\vec{\rho}_0-\vec{\rho}-\vec{\rho}_{mn}|^2+(|z_0-z'|+c)^2}}}{4\pi\sqrt{|\vec{\rho}_0-\vec{\rho}'-\vec{\rho}_{mn}|^2+(|z_0-z'|+c)^2}}\right|$$

$$+\frac{1}{CA}\sum_{m=-\infty}^{\infty}\sum_{n=-\infty}^{\infty}\int\tilde{T}(\beta_x,\beta_y,z')\int\tilde{J}(\beta_x,\beta_y,z')\frac{e^{-j\gamma|z_0-z'|+cCA}}{2j\gamma}dz'dz$$

The spatial domain integration is performed numerically. The spectral domain integration is performed analytically. When there is no overlap in $\hat{z}$ between $\tilde{J}$ and $\tilde{T}$, the spectral domain contribution becomes

$$\frac{1}{CA}\sum_{m=-\infty}^{\infty}\sum_{n=-\infty}^{\infty}\left|\frac{e^{-jA_1\frac{s}{2}}-e^{+jA_1\frac{s}{2}}}{-jA_1}\right|\left|\frac{e^{+j(\beta_x x_T+\beta_y y_T)}}{2j\gamma}\right|\left|\frac{e^{+j\gamma\left|\frac{\Delta_z}{2}-|z_T|\right|}-e^{-j\gamma\left|\frac{\Delta_z}{2}+|z_T|\right|}}{j\gamma}\right| \tag{3.20a}$$

With overlap the spectral domain contribution becomes

$$\frac{1}{CA}\sum_{m=-\infty}^{\infty}\sum_{n=-\infty}^{\infty}\left|\frac{e^{-jA_1\frac{s}{2}}-e^{+jA_1\frac{s}{2}}}{-jA_1}\right|\left|\frac{e^{+j(\beta_x x_T+\beta_y y_T)}}{2j\gamma}\right|\left|\frac{2-e^{-j\left|\frac{\Delta_z}{2}+z_T\right|}-e^{-j\left|\frac{\Delta_z}{2}-z_T\right|}}{j\gamma}\right| \tag{3.20b}$$

where

$A_1 \quad \beta_x\cos\theta+\beta_y\sin\theta$

Since the spectral and spatial domain contributions are integrated separately, the test point of the asymptotic terms must be fixed for the entire calculation. The asymptotic test point must not fall on the basis function since the singularity of the asymptotic term is not taken into account. Method 3 is the same as Method 2 with a point approximation for the spatial domain integral outside the core region (m-1:1,n-1:1).

Figures 3.7-3.10 show the calculation time needed for all three methods for various locations of testing functions. In all cases, Method 3 is fastest at the cost of accuracy.

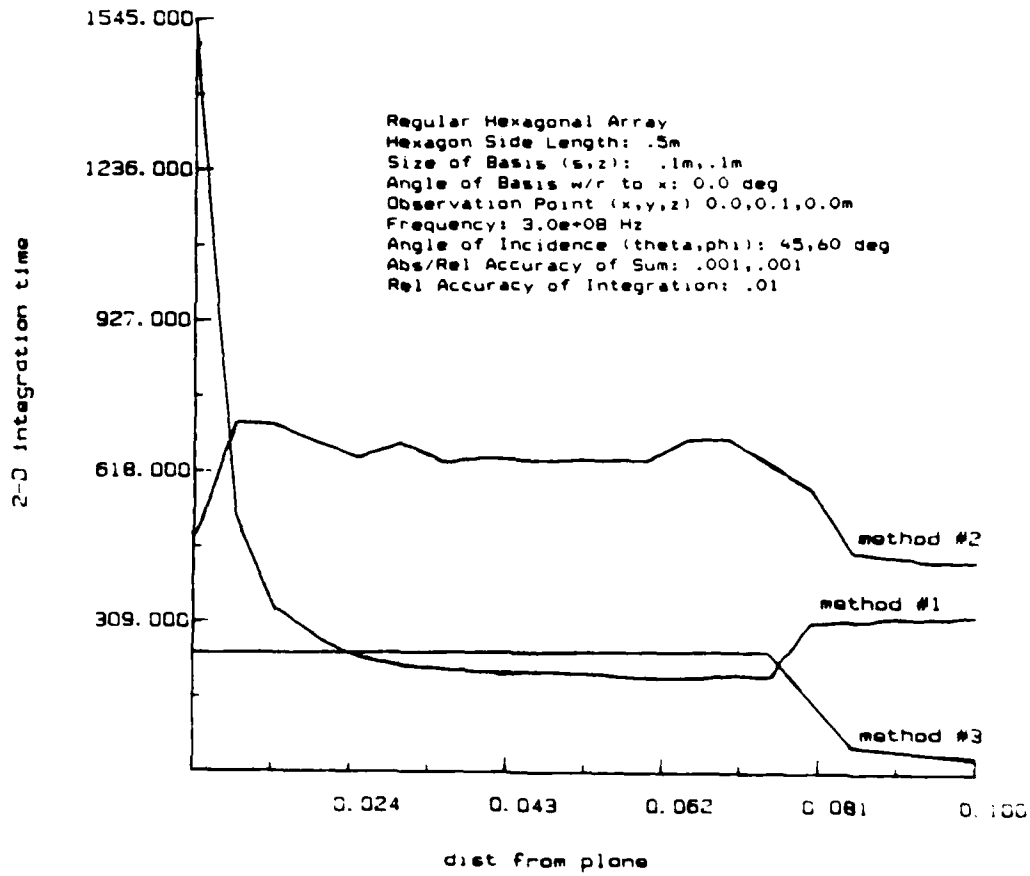

Figure 3.7 Time required for Methods 1,2 and 3 vs c for position 1 in Figure 3.11

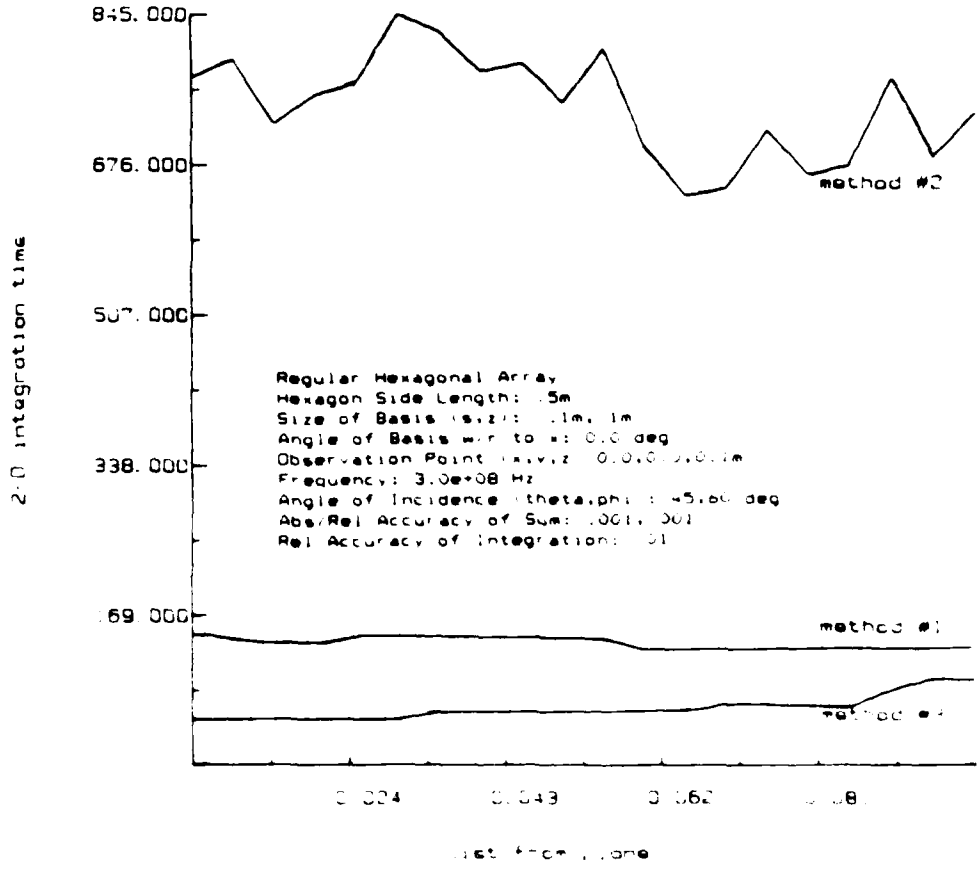

Figure 3.8 Time required for Methods 1,2 and 3 vs. θ for position 2 in Figure 3.11

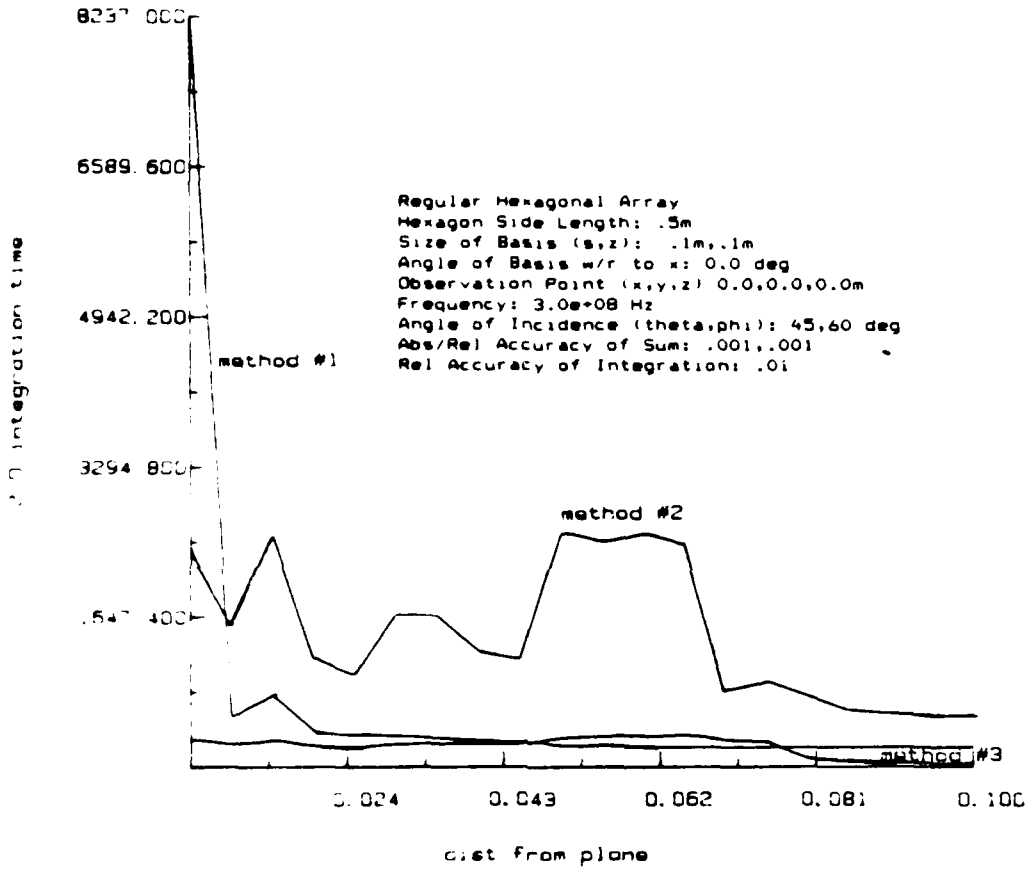

Figure 3.9 Time required for Methods 1,2 and 3 vs. c for position 3 in Figure 3.11

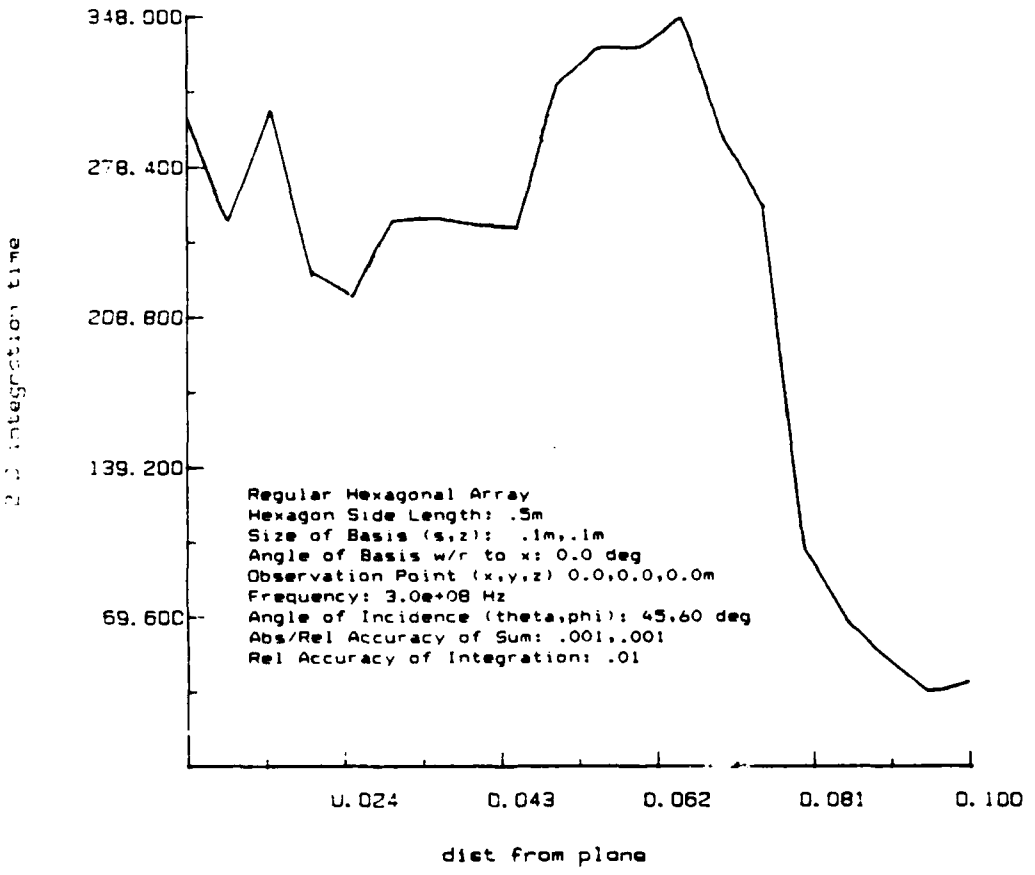

Figure 3.10 Time required for Method 3 vs. c for position 3 in Figure 3.11

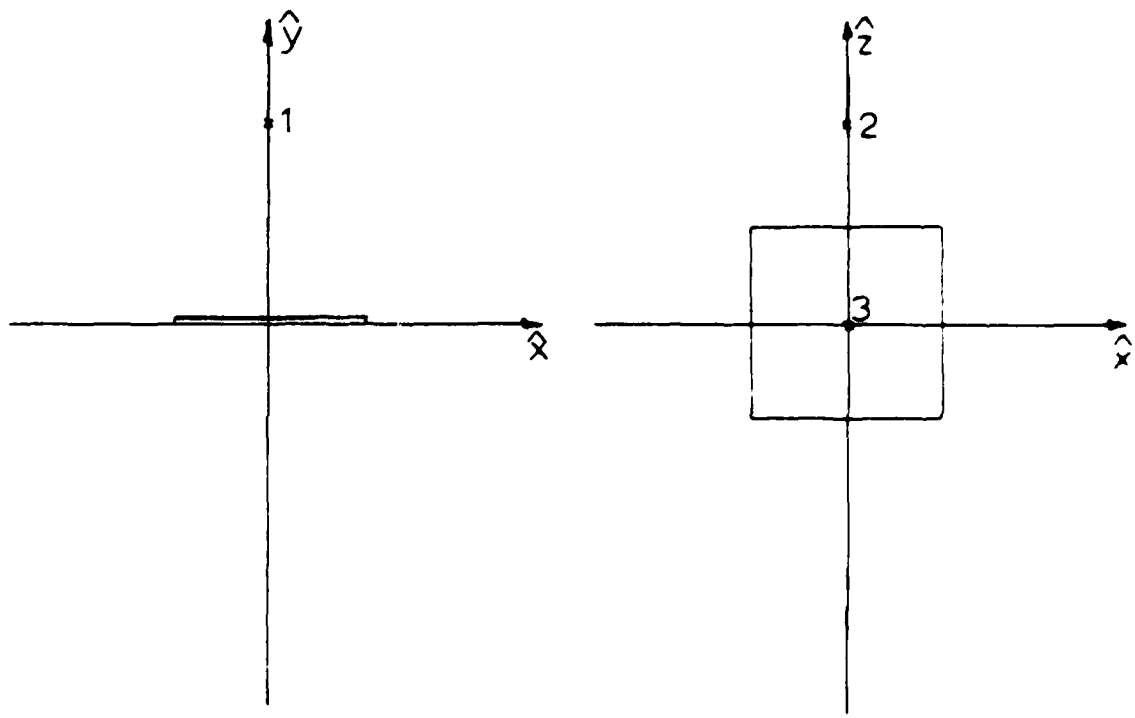

Figure 3.11 Positions of testing point for Figures 3.7-3.10

Method 1 is most accurate for all values of c. In Figure 3.7, the situation corresponds to 1 in Figure 3.11. Method 1 shows optimum time behavior in the $0.01 < c < 0.1$ range where weighting of spectral and spatial domain are approximately equal. Methods 2 and 3 show a drop in time at $c = 0.8$, where the spectral domain test point moves off plane and gets exponential convergence. Figure 3.8 corresponds to 2 in Figure 3.11. The test point is "off plane" to begin with. As a result, convergence for all methods is more rapid than in Figure 3.7. Figure 3.9 is the self term corresponding to 3 in Figure 3.11. The large times here arise from singularities in the asymptotic terms since until c exceeds 0.08, the testing point of the asymptotic term falls on the basis function. This can be seen more dramatically if Method 3 is examined alone (Figure 3.10).

4. CONCLUSIONS

This report has investigated the convergence characteristics of the periodic Green's function. The characteristics of the periodic Green's function have been discussed in the framework of two examples: (i) scattering from a one-dimensional array of strips, and (ii) scattering from a two-dimensional array of plates.

The periodic problem may be formulated in terms of responses to line/point sources (spatial domain) or in terms of response to current sheets (spectral domain). The spatial domain is slowly convergent everywhere while the spectral domain is only slowly convergent in the "on plane" case when the testing function is located in the array plane. The slow convergence in one domain stems from an unavoidable singularity in the reciprocal domain.

If the basis function is located entirely in the array plane (flat case), the derivatives may be transferred onto the Green's function and the smoothness of the basis and testing functions may be used to help convergence. If, on the other hand, the basis function is rotated in the array plane, then all derivatives in the expression must be transferred explicitly onto the basis and testing functions. The transfer of derivatives in the scalar potential term and approximations in the vector potential term simplify the problem to one of finding the response at a point due to an array of one-dimensional current pulses in the case of strips and two-dimensional current pulses in the case of plates.

In order to quickly do the summation to be computed in $T^R * J * G$, a combination of both the spectral and spatial domains must be used. Accelerating the spatial domain is shown symbolically as

$$T^R * J * \left[(G - G^a) + F^{-1}[\tilde{G}^a]\right] \tag{4.1}$$

The function G is slowly convergent but peaked. A smooth function that asymptotically approaches G (G^a) is subtracted from G to render the first two terms in the brackets rapidly converging. The function G^a is then added in the spectral domain using the Poisson

summation formula. Since the Poisson summation formula essentially Fourier transforms a smooth function with wide support, this term is also rapidly convergent. The same procedure may be applied to the spectral domain.

$$T^R * J * \left| F^{-1}(\tilde{G} - \tilde{G}^a) + G^a \right| \tag{4.2}$$

The function G^a in Equation (4.1) was chosen by moving the testing point "off plane" through use of a parameter c. In this report, c is multiplied by the area of the unit cell to get a distance. Numerical experiments were performed to determine the value of c required to minimize the time needed to calculate Equation (4.1). Three methods were studied: Equation (4.1) itself (Method 1); distributing the basis and test convolutions onto each domain and performing the convolution analytically in the spectral domain (Method 2); finally, calculating the out of core terms of the spatial portion of Method 2 using a point approximation to the integrals (Method 3).

Method 1 is the most accurate of all the methods for all values of c chosen. The optimum value of c for Method 1 is in the range $0.01 < c < 0.1$. For this range, the spatial and spectral domains are weighted approximately evenly. Method 3 is the least accurate of the methods and its accuracy decreases as c is increased, due to the approximation in the spatial domain. Method 3 is also the fastest method of the three for a wide range of c. The optimum value of c for Method 3 due to the accuracy is $0.001 < c < 0.03$. Method 2 has accuracy problems whenever the "on plane" case occurs. It is also the slowest of all the methods due to problems in specifying the absolute accuracy of the summations.

In summary, Method 1 is recommended when accuracy is the prime concern while Method 3 is recommended when speed is desired. In all cases, the choice of c must be made to ensure that the asymptotic term test point does not fall on the basis function since the singularity of the asymptotic term has not been taken into account.

In general, it was found that when the strips or plates are flat in the array plane, the smoothness and width of the basis and testing functions help the convergence of the

spectral domain so much that the spectral domain should get the entire weighting. Acceleration techniques need not be applied. In the cases where the strips or plates are rotated with respect to the array plane, acceleration techniques can be applied which results in a substantial time saving when c is selected in the ranges recommended above.

REFERENCES

[1] T. A. Cwik, "Scattering from general periodic screens," Ph.D. dissertation, University of Illinois, Urbana, IL, 1986.

[2] S. M. Wright, "Efficient analysis of infinite microstrip arrays on electrically thick substrates," Ph.D. dissertation, University of Illinois, Urbana, IL, 1984.

[3] R. W. Lampe, "A method of moments solution of strip-line discontinuity problems," Ph.D. dissertation, University of Illinois, Urbana, IL, 1984.

[4] R. C. Hall, "Electromagnetic scattering from periodic structures comprised of resistive sheet material," Ph.D. dissertation, University of Illinois, Urbana, IL, 1986.

[5] C. H. Tsao and R. Mittra, "Spectral-domain analysis of frequency selective surfaces comprised of periodic arrays of cross dipoles and jerusalem crosses," *IEEE Trans. Antennas Propagat.*, vol. AP-32, no. 5, pp. 478-486, May 1984.

[6] R. E. Collin, *Field Theory of Guided Waves*. New York: McGraw-Hill Co., 1960.

[7] R. Lampe, P. Klock, and P. Mayes, "Integral transforms useful for the accelerated summation of periodic, free-space Green's functions," *IEEE Trans. Microwave Theory Tech.*, vol. MTT-33, no. 8, pp. 734-736, August 1985.

[8] W. F. Richards, K. McInturff, and P. S. Simon, "An efficient technique for computing the potential Green's functions for a thin, periodically excited parallel-plate waveguide bounded by electric and magnetic walls," *IEEE Trans. Microwave Theory Tech.*, vol. MTT-35, no. 3, pp. 276-281, March 1987.

[9] N. G. Alexopoulos and I. E. Rana, "Mutual impedance computation between printed dipoles," *IEEE Trans. Antennas Propagat.*, vol. AP-29, no. 1, pp.106-111, Jan. 1981.

[10] R. Gabel and R. Roberts, *Signals and Linear Systems*. New York: Wiley and Sons, 1973.

[11] C. Kittel, *Introduction to Solid State Physics*. New York: Wiley and Sons, 1976.

[12] A. W. Glisson and D. R. Wilton, "Simple and efficient numerical methods for problems of electromagnetic radiation and scattering from surfaces," *IEEE Trans. Antennas Propagat.*, vol. AP-28, no. 5, pp. 593-603, Sept. 1980.

END

10-81

DTIC